The growth of faults and fracture networks in a mechanically evolving, mechanically stratified rock mass: A case study from Spireslack Surface Coal Mine, Scotland

Billy J. Andrews*, Zoe K. Shipton, Richard Lord, Lucy McKay

Department of Civil and Environmental Engineering, University of Strathclyde, Glasgow, G11XJ, Scotland

Correspondence to: Billy J. Andrews (billy.andrews@strath.ac.uk)

Abstract.

Fault architecture and fracture network evolution (and resulting bulk hydraulic properties) are highly dependent on the mechanical properties of the rocks at the time the structures developed. This paper investigates the role of mechanical layering and pre-existing structures on the evolution of strike-slip faults and fracture networks. Detailed mapping of exceptionally well exposed fluvial-deltaic lithologies at Spireslack Surface Coal Mine, Scotland, reveals two phases of faulting with an initial sinistral, and later dextral, sense of shear with ongoing pre-, syn- and post-faulting joint sets. We find fault zone internal structure depends on whether the fault is self-juxtaposing or cuts multiple lithologies, the presence of shale layers which promote bed-rotation and fault-core lens formation, and the orientation of joints and coal cleats at the time of faulting. During ongoing deformation, cementation of fractures is concentrated where the fracture network is most connected. This leads to the counter-intuitive result that the highest fracture density part of the network often has the lowest open fracture connectivity. To evaluate the final bulk hydraulic properties of a deformed rock mass it is crucial to appreciate the relative timing of deformation events, concurrent or subsequent cementation, and the interlinked effects on overall network connectivity.

1 Introduction

Differences in the mechanical properties (mechanical stratigraphy) of rock layers have long been recognised as influencing the style and evolution of faults (Anderson, 1951; Donath, 1961; Ranalli and Yin, 1990; Ferrill et al., 2017)). However, work has tended to focus particularly on normal faults, with the effect of mechanical layers in sand-shale sequences (e.g. van der Zee & Urai (2005); Schmatz *et al.* (2010)), interbedded limestones and marls (e.g. Ferrill & Morris (2003), (2008); Long & Imber (2011); Ferrill *et al.* (2012)), and ignimbrites (Soden and Shipton, 2013) receiving particular attention. The lithology being cut by the fault influences fault dip, e.g. strands in competent layers have steeper dips than those in incompetent layers (Ferrill and Morris, 2008), with important consequences for vein geometry and mineralisation potential (Dunham 1948). The ratio of competent to incompetent lithologies thus affects fault style and displacement profiles (Ferrill et al., 2017; Ferrill and Morris, 2008). Fault-related folding of thin competent layers (e.g. limestones) is common in successions otherwise dominated by incompetent lithologies (e.g. shale) (Ferrill and Morris, 2008; Lăpădat et al., 2017). The presence of incompetent lithologies also restricts fault growth with strands terminating at incompetent beds and leads to formation of faults with high length to height ratios orientated parallel to the strike of bedding (e.g. Nicol *et al.* (1996); Soliva & Benedicto (2005); Roche *et al.* (2013)).

Pre-existing weaknesses (e.g., joints and faults) also play an important role in the nucleation, orientation, and length of later faults (Crider and Peacock, 2004; Peacock, 2001; Walsh *et al.*, 2002). The mechanical response of a pre-existing joint to faulting will depend on its orientation relative to far field stress (Moir et al., 2010), the ratio of principal stresses (Lunn et al., 2008; Healy et al., 2006; Moir, 2010; Chang and Haimson, 2000; Haimson and Chang, 2000), and local variations in the stress field due to the interaction of joints in the pre-existing network (Crider and Peacock, 2004; Kattenhorn et al., 2000; Moir et al., 2010; Peacock, 2001). Where joints or cleats are orientated perpendicular to the growth direction of faults, they can act as a strength contrast and restrict fault growth (Wilkins and Gross, 2002). Alternatively, where pre-existing joints are orientated favourably, they can act as a plane of weakness and be reactivated to form faulted joints (e.g. Crider and Peacock, 2004; Cruikshank et al., 1991; Wilkins et al., 2001).

Veins are often associated with faulting, providing evidence of the paleo-fluid flow through a fracture network (Bons et al., 2012; Oliver and Bons, 2001; Peacock and Sanderson, 2018) and may act as a baffle to post-cementation basinal fluid flow (e.g. Skurtveit et al., 2015). Additionally, the strength of a rock mass can vary depending on the strength ratio between the host-rock and veins, along with the mineralogy, thickness, and orientation of veins relative to the maximum compressive stress (e.g. Shang et al., 2016; Turichshev and Hadjigeorgiou, 2016, 2017; Virgo et al., 2014). Therefore, the cementation

of faults and joints can influence subsequent deformation of the rock mass (Caputo and Hancock, 1998; Holland and Urai, 2010; Ramsay, 1980; Virgo et al., 2013, 2014).

This study utilises an exceptional succession of faulted fluvial-deltaic exposures of the Limestone Coal Formation exhumed at the Spireslack Surface Coal Mine, Scotland. Coal-bearing, fluvial-deltaic sequences are commonly mechanically stratified. Fluvial-deltaic sequences are characterised by cyclical sequences of limestone, sandstone, siltstone, seat-earth (paleosols that are often found beneath coal seams), shale and coal (Thomas, 2013, *and references therein*). The competent lithologies in the sequence (limestone and sandstone) commonly contain joints. Coal has a distinctive blocky texture due to the presence of two roughly perpendicular fracture sets referred to as cleats (Laubach et al., 1998). Cleats form in coal beds during diagenesis and act as pre-existing weaknesses that can influence the location, orientation and length of faults. We investigate how the internal structure of strike-slip faults at Spireslack Surface Coal Mine depends on the lithology, presence of pre-existing weaknesses (e.g., joints, cleats) and synchronous cementation. Our observations contrast small offset, self-juxtaposing faults and faults with larger offsets that cut multiple lithologies.

2. Geological setting

Spireslack Surface Coal Mine is located in the Midland Valley of Scotland, a 90 km wide, 150 km long, ENE-trending basin that opened during the late Devonian to Early Carboniferous in response to back-arc extension within the Laurussian Plate (Leeder, 1982, 1988). This was followed by a period of thermal subsidence which continued throughout Namurian and Westphalian times leading to the deposition and preservation of thick coal measures across much of the UK (Figure 1a) (Leeder, 1982).

The Midland Valley is bound by two major faults; the Southern Upland Fault to the south and Highland Boundary Fault to the north (Figure 1a) (Bluck, 1984). Carboniferous basins that have axes oblique to the main trend of the Midland Valley (e.g. Central Scottish Coalfield; Francis (1991)) can reach over 6 km in thickness (Dean et al., 2011). Faults with associated, localised folding have a complex history of reactivation caused by sinistral strike-/oblique-slip movement during the Tournaisian and dextral strike-/oblique-slip movement during Viséan to Westphalian times (Browne and Monro, 1987; Rippon et al., 1996; Ritchie et al., 2003; Underhill et al., 2008).

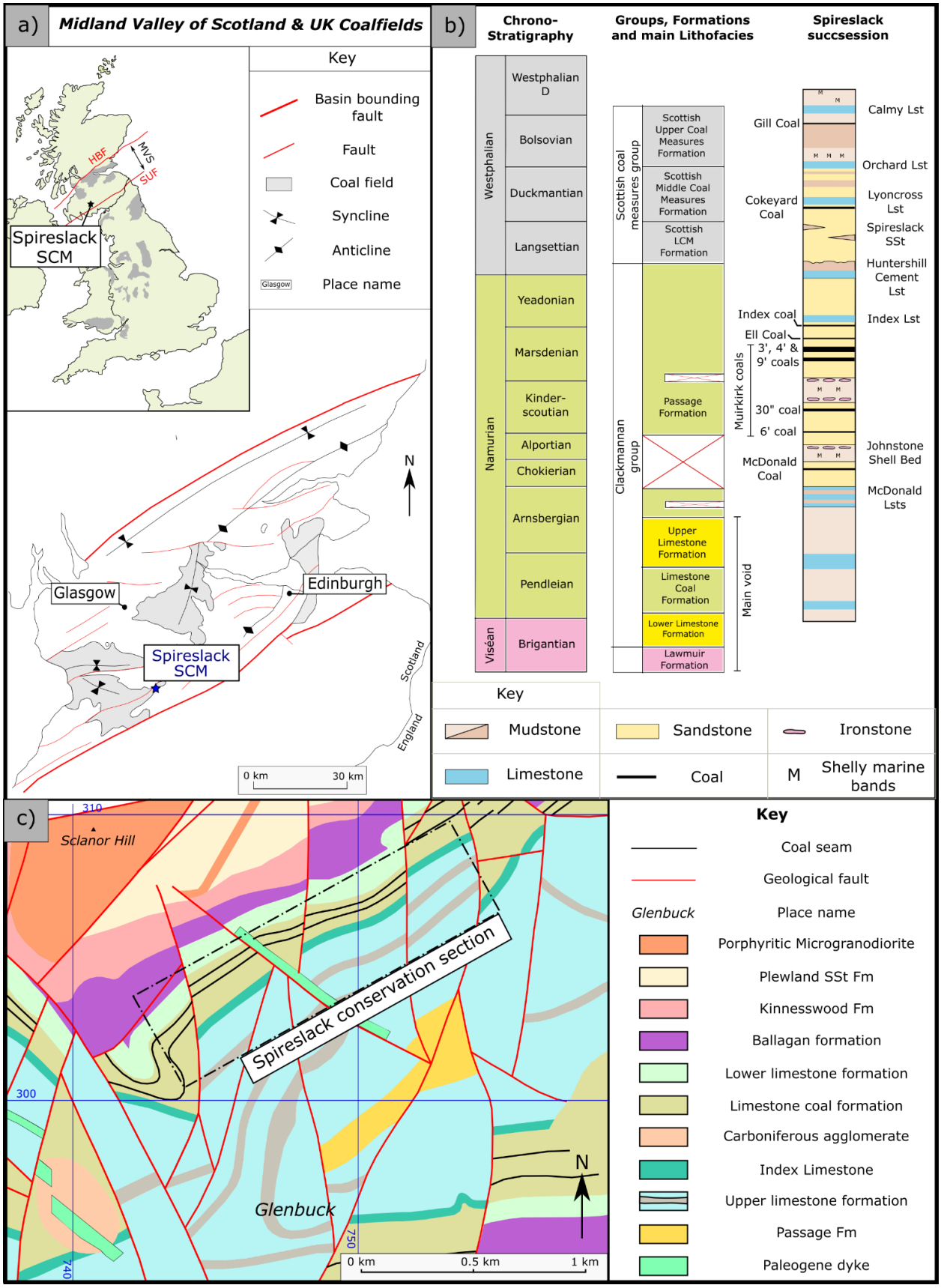

Figure 1: Location map: a) Map of UK coalfields (adapted from Donnelly (2006)) showing the location of Spireslack Surface Coal Mine (SCM) and structural features of the Midland Valley of Scotland; b) Regional geology and c) stratigraphy of Spireslack open cast coal mine (after Ellen et al. (2019)).

2.1 Spireslack Surface Coal Mine

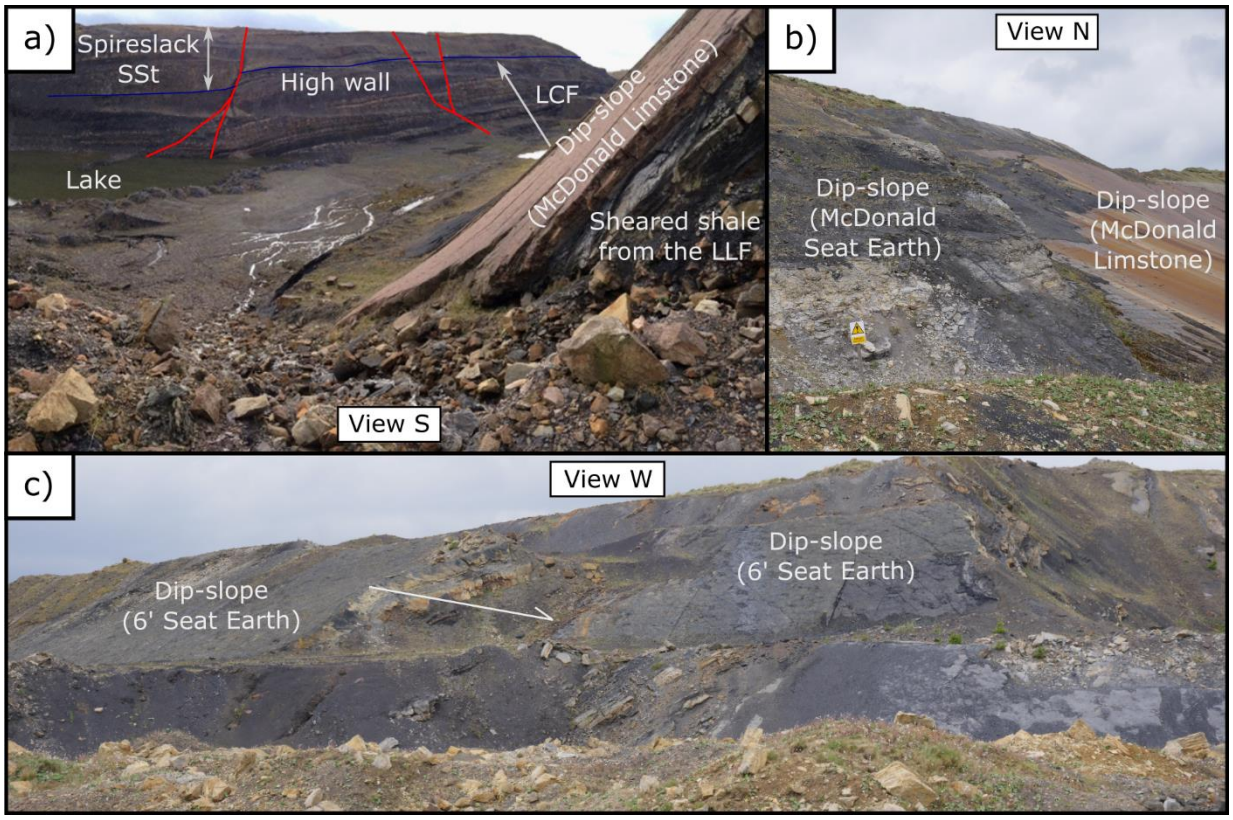

Figure 2: Overview photographs of Spireslack SCM: a) Photograph from the east of the site of the high wall with the McDonald Limestone dip slope visible to the right in the foreground; b) photograph looking down the McDonald Limestone pavement from the entrance roadway c) Photograph of the 6' Seat Earth exposed in the dip-slope to the west of the site.

Spireslack Surface Coal Mine (SCM), next to the now abandoned coal mining village of Glenbuck in South Ayrshire, Scotland (Figure 1a) provides an exceptional exposure of Carboniferous rocks in a 1 km long residual void (Figure 2 & 1c). Shallow, southerly dipping (20°- 40°) bedding planes (dip-slopes) end in a <130 m high working face (the high wall) (Figure 2). The high wall represents the unexcavated working face exposed through the opencast operations, with bedding planes (e.g. the McDonald Limestone) used as the void's dip-slopes.

The stratigraphy is comprised of a continuous succession of Viséan to Namurian strata, including a complete section through the Limestone Coal Formation (LCF) (Figure 1b, c) (Ellen et al., 2016, 2019). Bitumous coal is found in cyclical fluvio-deltaic sequences that outcrop across much of the dip-slope and high wall, bounded by the Upper and Lower Limestone Formations. The Lower Limestone Formation represents more marine-influenced facies including extensive, fossil-rich limestone units (e.g. the McDonald Limestone) (Davis, 1972). The Spireslack Sandstone is exposed above the Limestone Coal Formation and comprises of one channelised and two tabular sandstone beds (Ellen et al., 2019).

Several faults with shallow slip vectors and variably complex internal structures offset the stratigraphy. Additionally, at least five Paleogene basaltic dykes are observed trending NW-SE to WNW-ESE, which Leslie *et al.* (2016) suggest intrude along pre-existing faults. The rocks exposed at Spireslack SCM are part of the southern limb of the upright, WSW-ENE trending Muirkirk syncline that formed in response to mid- to late- Carboniferous sinistral transpression (Davis, 1972; Leslie et al., 2016). Leslie *et al.* (2016) attribute the faulting and folding observed at Spireslack SCM to this deformation, and have observed no evidence at the site of the later widespread dextral deformation found elsewhere in the Midland Valley (e.g. Underhill *et al.* (2008)).

3. Methods

3.1. Field mapping

Geological mapping of the dip-slopes captured all sandstone and shale units below the McDonald Limestones and the sandstone bed above the Muirkirk 6' Coal. Mapping was undertaken at a 1:1,000 scale onto printed aerial photography from Bing Maps (Microsoft, 2017). All faults with >0.2 m stratigraphic separation were recorded. When considering the effect of lithology on fault structure we attempt to apply the terminology used in fault sealing studies in which a self-juxtaposing fault is a fault where the offset is small enough with respect to the layer thickness that the same layer is present on either side (e.g. Gibson and Bentham, 2003; Knai and Knipe, 1998; Pei et al., 2015; Yielding et al., 2011). Printed field photographs were used to collect more detailed observations at several key sites.

3.2 Lineament mapping and network analysis

One way to describe the topology of a fault or fracture network is as a series of branches and nodes (e.g. Manzocchi 2002; Sanderson & Nixon, 2015; 2018). A branch is a fracture trace with a node at each end. Nodes can occur where a fracture terminates into rock (I-node), abuts against another fracture (Y-node) or crosses another fracture (X-node). The proportion of different node types (I, Y, and X) can then be plotted on a triangular diagram to characterise the connectivity of the network (Manzocchi, 2002; Sanderson and Nixon, 2015). In this work we recorded faults and fractures as orientation sets and report fracture/branch trace length (tl), 2D fracture intensity (I), and the percentage of connected branches (Pc, see Equation 1).

Fault and fracture mapping were undertaken using two datasets: (i) a drone derived photomontage of the McDonald Limestone bedding plane provided by Dave Healy of Aberdeen University; and (ii) an auto-rectified photomontage of the high wall collected by the British Geological Survey. In order to understand the geometry, topological properties and crosscutting relationships of fault strands/joint sets,

interpretation areas were selected from both the dip-slope and high wall for analysis. Due to its instability the high wall is generally unsafe to access, so any interpretations of the high wall are made principally on the photomontage. We outline our workflow in detail below:

1. *Lineament mapping:* Field mapping was undertaken by the lead author at a scale of 1:30 for the dip-slope and 1:50 for the high wall. Scanned field maps were georeferenced and scaled in ArcGIS. Digitisation of the mapped lineaments, and correlation of features between well exposed areas, was undertaken by the same person to limit the effect of subjective bias (Andrews et al., 2019; Scheiber et al., 2015). The faults and the fractures were digitised into separate GIS layers, with reference to field notebooks and maps to ensure interpretations honoured the field data. While in the detailed field investigation areas it was possible to distinguish shear fractures from joints, this was not possible for much of the area. Therefore, both potential shear fractures and joints were included in the 'joint' dataset when in inaccessible areas. The fault and joint datasets were then merged in ArcGIS, to create a third dataset: the 'combined network'. The fault, joint, and combined datasets were then investigated separately, using a network analysis outlined in steps 2 to 4.
2. *Define sets:* Six 'interpretation boxes' that cover a range of deformation styles and fracture intensity were defined as shape files in ArcGIS (three along the dip-slope and three along the high wall). The orientation of faults and fractures within them were then analysed. Length-weighted rose diagrams with 5° bin widths were used to interpret the orientation sets in the network using the NetworkGT toolbox (Nyberg et al., 2018).
3. *Branch & Nodes:* The topology of the network was then extracted using the 'Branch and Node' tool in NetworkGT, which splits the fracture trace poly-line file into individual branches, and assigns I, Y or X nodes as a separate point-files (Nyberg et al., 2018). The resulting network was visually checked for errors (e.g. incorrectly assigned nodes) and manually adjusted in ArcGIS to remove spurious nodes and branches. Data were then exported to Excel for further analysis.
   The digitisation and analysis of the fault network separately from the 'joint' dataset meant that where faults terminated against pre-existing joints (i.e. a y-node in the combined network), this was classified as an isolated node. This was done to provide the network properties (i.e. connectivity, trace length and fracture intensity) of the 'active' fault network where evidence of shear and mineralisation is present. Because the mineralised fault network will be sealing to flow, and therefore not hydrologically connected to the joint network, it is not appropriate to classify joint-fault abutting relationships as connected nodes. Therefore, where a joint terminates against a pre-existing fault in the 'joint' dataset this was also classified as an i-node. The combined network represents the fault-fracture network that is typically digitised and analysed for topological analysis.

4. *Network analysis:* For each network, the following data were extracted;

   a. *Network connectivity:* For each dataset, with the data not split into sets, the node and branch proportions were assessed using a triangular diagram (c.f. Sanderson & Nixon (2015)). From the number of I (N_i), Y (N_y)and X (N_x) nodes, the proportion of connected branches was then calculated using Equation 1 (Sanderson and Nixon, 2015):

$$P_c = \frac{(3N_y+4N_x)}{(N_i+3N_y+4N_x)} \qquad \text{(Equation 1)}$$

   b. *Trace length:* The trace length of digitised networks and sets within each sample area were assessed using trace length distributions (Priest and Hudson, 1981), with the minimum, maximum, and median trace length values used to compare analysis.

   c. *2D fracture intensity:* We compared the intensity of the networks and sets within the network using 2D fracture intensity (Equation 2) (P_{21}; Dershowitz & Einstein (1988); Rohrbaugh *et al.* (2002)).

$$P_{21} = \frac{\sum L}{A} \qquad \textit{(fractures / m)} \qquad \textit{(Equation 2)}$$

$$\sum L = sum\ of\ all\ fracture\ trace\ lengths, A = sample\ area$$

4. Fault and fracture observations

4.1 General fracture observations

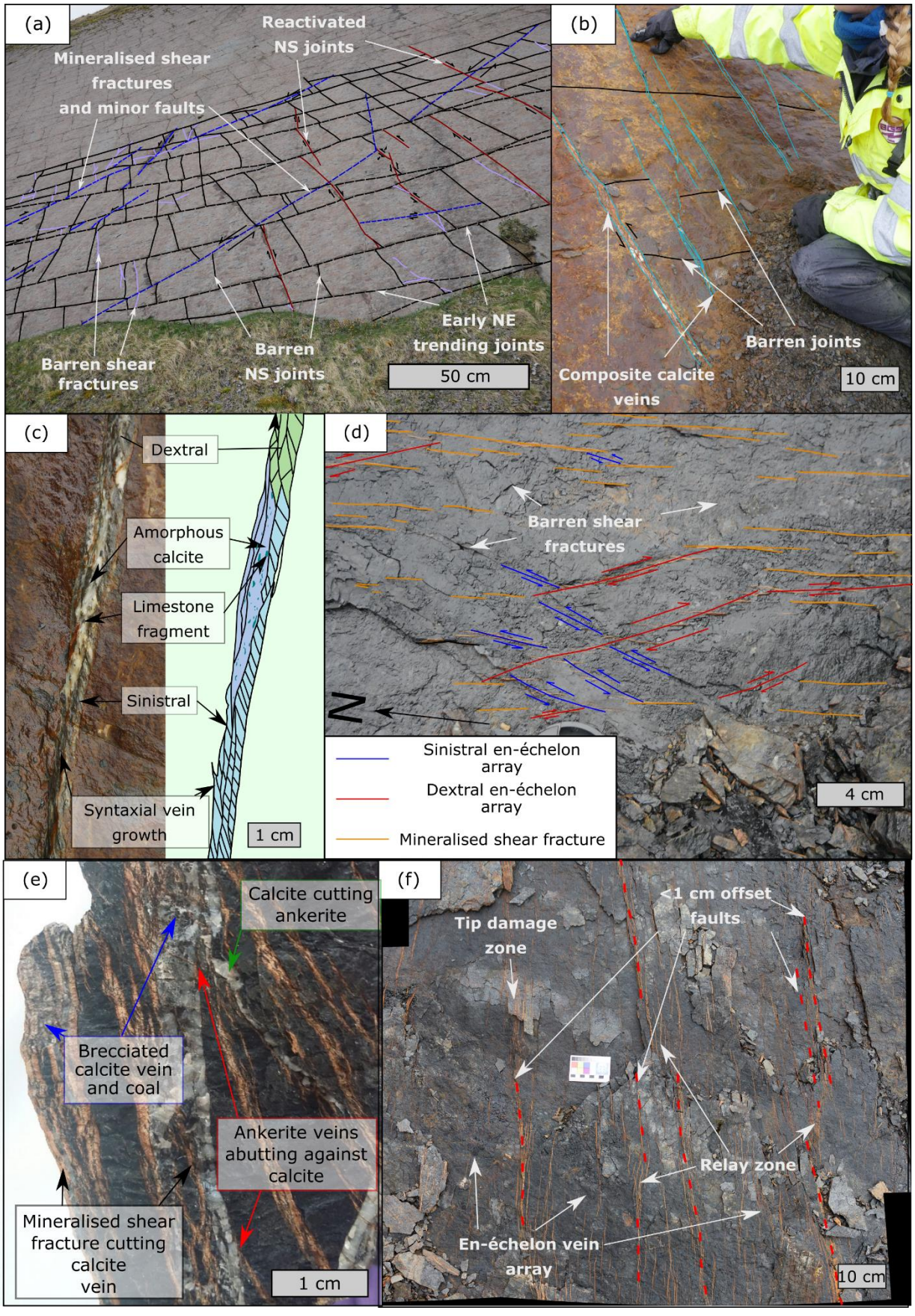

Figure 3: Typical fracture properties for McDonald Limestone & McDonald Coal: a) joints observed away from faults across the southerly dipping (c. 40°) McDonald Limestone bedding plane; b) Mineralised N-S trending calcite veins, offsetting abutting E-W ladder joints on the bedding plane of the McDonald Limestone; c) annotated field photograph and interpretation of a multi-phase composite calcite vein exposed in the vicinity to a small stratigraphic separation fault along the McDonald Limestone Pavement; d) bedding plane exposure of mineralised fractures present within the Muirkirk 6' coal; e) annotated hand specimen displaying the vein relationships present during the faulting of the Muirkirk 6' coal; and f) the larger-scale mineralisation pattern as you move towards small stratigraphic separation faults in the Muirkirk 6' coal.

Fractures at Spireslack SCM can be classified as either joints (barren open mode fractures), faulted joints (joints that show evidence of reactivation, E.g., mineralisation or cataclasis) , or shear fractures, with the latter two often found in proximity to faults. In this study 'shear fractures' refer to a fracture with displacement below map scale and can be either mineralised or barren. Crosscutting relationships are often complex and display several age sets. For example, in the McDonald Limestone bedding plane (Figure 3a) there are two generations of joints: an early set of NE-SW trending joints (dashed black in Figure 3a) and a later set of N-S trending joints (black) that abut the earlier set. Both generations represent the pre-existing fracture set at the time of faulting. These pre-existing joints are then cut by a set of NNE-SSW trending mineralised shear fractures (dashed blue) that are restricted by favourably orientated joints and are locally are associated with new barren shear fractures (lilac). Finally, several of the N-S trending joints become reactivated (maroon) and are interpreted as faulted joints (c. Zhao and Johnson, 1992).

Calcite mineralisation at Spireslack SCM (Figure 3b, c), which is often found associated with faults, occurs as two styles: 1) amorphous, where no growth structures are present and occasional fragments of limestone are observed within the vein, or 2) with syntaxial growth textures suggesting both sinistral and dextral motion during the mineralisation of a single vein (Figure 3c). Along fault planes and within a few meters of faults, composite veins commonly occur, with multiple growth stages and evidence of reactivation (Figure 3c).

Fractures in the coal layers are commonly filled with a buff to orange coloured mineral, identified in the field as ankerite (iron rich carbonate) (Figure 3d-f). Fractures in coal occur as:

- *Coal cleats:* Ubiquitous in all coals, cleats are orthogonal opening mode fractures that develop during burial diagenesis (Laubach et al., 1998). Cleat spacing (typically <2 cm) is dependent on bed-thickness, coal quality and the presence of clastic material (e.g. shale partings).
- *Mineralised shear fractures:* Typically 2 to 15 cm long, but increase to greater than 1 m long as stratigraphic separation increases. Fractures less than 15 cm long abut against E-W trending

cleats, with trace length restricted by cleat spacing. Longer fractures cut through the cleats. The thickness of planar ankerite veins increases with the length of the vein.

- *En-echelon arrays:* En-echelon ankerite veins display both sinistral and dextral motion (Figure 3d). Dextral arrays can occur both simultaneously with, or later than, sinistral arrays.
- *Barren shear fractures:* In addition to the cleat network, fractures that abut against all other fractures are often curved and have trace lengths typically between 5 to 15 cm. These may propagate from the tip of pre-existing mineralised shear fractures (Figure 3d).

Other lithologies observed in Spireslack SCM display a strongly developed fracture stratigraphy (c.f. Laubach *et al.* (2009)). For example, the McDonald Seat Earth exposed in the dip-slope towards the west of the site (Figure 4a), lacks a well-developed joint pattern. Instead, shear-fractures are observed in relation to small stratigraphic offset, strike-slip faults (Figure 5a,b). Fractures are only found in close proximity to fault strands and are either sub-parallel to fault strands in the hanging wall block, or oblique to the fault strands in relay zones and fault tips. Fractures commonly display small sinistral and dextral stratigraphic offsets (mm to cm) and are typically barren, although occasionally pyrite is found along the fracture plane. Sandstones display bed-bound joint-sets in a similar manner to the McDonald Limestone. However, there was limited bed-parallel exposure to explore the age and orientation of fracture sets in sandstone lithologies. In contrast to the dip-slope, seat-earth in the high wall displays a well-developed bed-bound fracture network. This suggests that mine-related stresses may have caused deformation of these lithologies and that the natural network has been altered by both subsurface and surface mining activities.

4.1.1. Order of fractures within the Muirkirk 6’ coal

Like the McDonald Limestone bedding plane (Figure 3a-c), a complex chronology of fractures can be observed in the Muirkirk 6’ coal (Figure 3d-f). In Figure 3d, dextral en-echelon vein arrays (red) crosscut earlier sinistral sets (blue), with the former abutting against mineralised shear fractures. Barren shear fractures then abut against both sets displaying a curvature indicative of a dextral fracture array. Abutting relationships suggest the barren shear fractures likely formed at the same time as the dextral en-echelon vein array; however, given the lack of mineralisation it is likely they were isolated from the source of mineral rich fluids.

In Figure 3e, multiple phases of mineralisation and reactivation of veins can be observed. Veinlets of ankerite both abut against, and cut through, the calcite vein associated with a nearby small (<5 cm) stratigraphic offset fault. Brecciation of coal and calcite is also observed, with undisrupted ankerite

256 veinlets cutting through the breccia. This requires a minimum of four stages of
257 mineralisation/deformation:

258 1) Ankerite veinlets formed along the N-S striking face-cleats.

259 2) Faulting led to the development of coal breccia and calcite veining which either cut across or
260 abut against pre-existing structures.

261 3) Brecciation of the calcite vein and coal led to the development of a chaotic fault breccia
262 (following the classification of Woodcock and Mort (2008)). The breccia contains angular clasts
263 of coal and calcite within an amorphous calcite matrix.

264 4) Finally, mineralisation returned to ankerite with dextral en-échelon arrays developed
265 alongside barren tip-damage zones.

266 These observations suggest that initial deformation and associated mineralisation occurred over a wide
267 zone of en-échelon arrays (Figure 3d), which was strongly influenced by the pre-existing cleat network
268 (Figure 3e). En-échelon arrays then began to interact leading to the development of localised
269 mineralised shear fractures (Figure 3f). As the trace length of the shear fracture increased, so did the
270 thickness of the zone leading to the formation of a dense array of small stratigraphic offset (<1 cm)
271 strands which interacted through the development of relay-zones. A later dextral stress state,
272 demonstrated by reactivated features (Figure 3e), lead to another phase of en-echelon vein formation
273 (Figure 3c), which also locally developed into mineralised shear fractures.

274 **4.2 Fault observations**

275 In order to understand the role of lithology on faulting style we describe and compare fault
276 characteristics between faults that cut the same lithology (self-juxtaposing faults) and faults that
277 juxtapose multiple lithologies of the stratified sequence. Additionally, in order to elucidate the role of
278 pre-existing joints on faulting style, we focus on the interaction between faults and fractures within the
279 McDonald Limestone formation because of exceptional, laterally extensive bed-parallel exposure on the
280 dip-slope.

281 Faulting at Spireslack SCM formed either under early sinistral (Phase 1) or late dextral (Phase 2) shear
282 (Figure 4c). Phase 1 dextral faults are interpreted as having formed concurrently with normal faults in
283 the 6' Seat Earth and thrusts in the shale. The south-dipping bedding, is consistent with the regional fold
284 axis inferred from BGS maps (040°/80° N) also fits within the sinistral phase of deformation. Faulting

that cuts the earlier structures (e.g. the oblique sinistral fault and NW trending dextral fault strands) does not fit within the expected fault geometries of Phase 1 faults, and likely formed under a later period of dextral shear (Phase 2) (Figure 4c). In addition to the two phases of strike-slip tectonics, dykes (probably Paleogene) exploit pre-existing N-W trending fault strands. These locally display pods of edge brecciation similar to that developed along faults in limestone, and show dip-slip lineations suggesting there could have been a late stage of normal faulting.

4.2.1 Self-juxtaposing faults

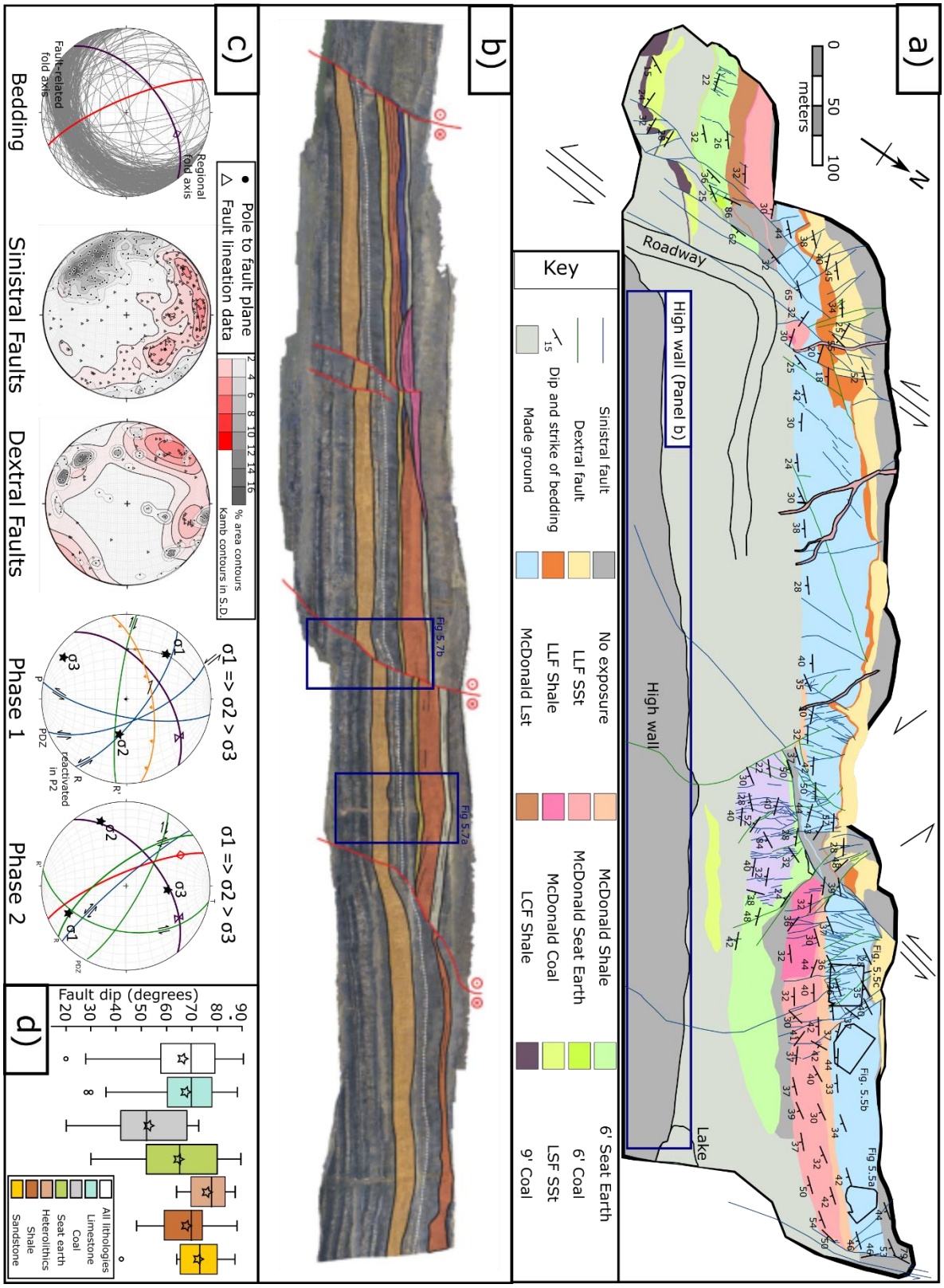

Figure 4: Geological map of Spireslack SCM: a) geological map undertaken as part of this study, displaying the locations of the detailed map-view fracture maps shown in Figure 8; b) annotated photogrammetry of the high wall displaying the key stratigraphic horizons and faults (Ellen et al., 2019); c) fault kinematics by lithology. Stereographic projections were created using Stereonet 10.1 and contours represent 1% area; and d) box and whisker plots for fault dip by lithology.

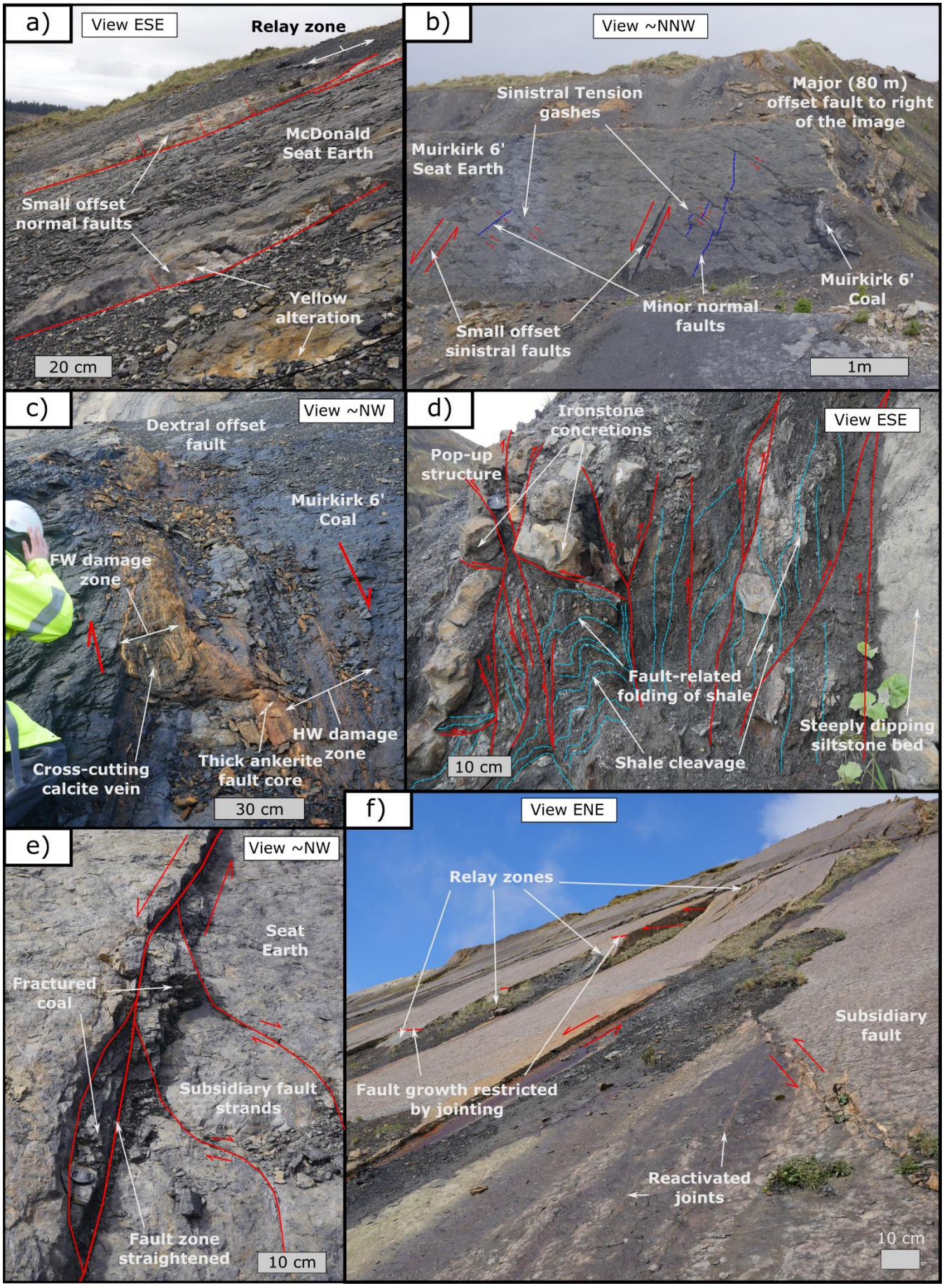
a)
View ESE
Relay zone
McDonald Seat Earth
Small offset normal faults
Yellow alteration
20 cm
b)
View ~NNW
Sinistral Tension gashes
Major (80 m) offset fault to right of the image
Muirkirk 6' Seat Earth
Muirkirk 6' Coal
Minor normal faults
Small offset sinistral faults
1m
c)
View ~NW
Dextral offset fault
Muirkirk 6' Coal
FW damage zone
HW damage zone
Thick ankerite fault core
Cross-cutting calcite vein
30 cm
d)
View ESE
Ironstone concretions
Pop-up structure
Fault-related folding of shale
Steeply dipping siltstone bed
Shale cleavage
10 cm
e)
View ~NW
Seat Earth
Fractured coal
Subsidiary fault strands
Fault zone straightened
10 cm
f)
View ENE
Relay zones
Subsidiary fault
Fault growth restricted by jointing
Reactivated joints
10 cm

298

Figure 5: Characteristic observations of Self Juxtaposed Faults (SJFs): a) Small stratigraphic offset (c. 15 cm) fault strands and relay structures, and b) tension gashes and small stratigraphic offset normal faults exposed within the McDonald Seat Earth in seat-earth exposed to the far west of Spireslack SCM; c) symmetric damage zone and thick zone of ankerite mineralisation along a c. 40 cm stratigraphic separation dextral fault cutting the Muirkirk 6' Coal [FW = Footwall, HW = Hanging wall]; d) bed-parallel thrusts and folding developed within the shale which underlies the McDonald Limestone to the NE of the site; e) the development of small pods of fractured McDonald Coal along a small stratigraphic offset sinistral fault exposed to the SW of the site; f) the interaction between faults and joints along the southerly dipping bedding plane of the McDonald Limestone.

Self-juxtaposing faults, with small stratigraphic offset (<3 m), form either isolated strands (e.g. west of the void) or a network of sinistral and dextral strands (e.g. near the centre of the void) (Figure 3). The internal structure of self-juxtaposing faults depends on the lithology that the fault strand cuts (Table 1, Figure 4). Self-juxtaposing limestones behave in a predominantly brittle manner with a fracture network decreasing in intensity away from the fault. Whereas, shale behaves in a more ductile manner and can lead to considerable bed-rotation and bed-parallel folding adjacent to the fault.

The fault dip depends on the lithology cut by the fault. Dips in the McDonald Limestone range from 45° to 88° (mean = 69.1°, n = 47), however, in coal seams fault dips range from 20° to 73° (mean = 49°, n = 24). In the shale interbeds, layer bound, bed-parallel thrusts (e.g. 040°/70° SE) with cm- to m-scale stratigraphic offsets and associated folding can be picked out where they cut ironstone layers (Figure 5d). The McDonald Seat Earth in the west of the site displays dip-slip slickensides (50° to 60°), but only in faults with stratigraphic separation <1 m.

Lithology	Self-juxtaposing fault characteristics
McDonald Seat Earth	Segment linkage, folding, and increased fracturing between strands led to the development of a highly asymmetric damage zone (Figure 5a, b, e). Faults typically barren, only displaying yellow alteration and occasionally pyrite.
McDonald Limestone	Self-juxtaposing faults, associated relay zones, and nearby N-S trending joint sets, are mineralised (calcite), display high displacement to length ratios (2.4 to 2.8), and show extensive folding of the surrounding lithologies (Figure 5f). Strands often abut against favourably orientated pre-existing joints.
Coal	Fault strands are characterised by a fault core comprising of a 5 to 20 cm thick zone of ankerite, with occasional calcite mineralisation, brecciated coal and pyrite (Figure 5c). The fault core is discontinuous along strike, with displacement transferring to other strands after 1 to 5 meters (Figure 5c). The gentle folding of the bed between strands is taken up by a symmetric zone of damage consisting of increased fracturing, en-echelon veining and mineralised shear fractures. The structures represent a continuation of the processes discussed in Section 4.1.1.
Shale	Fault strands are rarely observed. High angle thrusts (40° to 60°) dominate, with bed parallel folding picked out by ironstone concretions (Figure 5d), which themselves can display internal deformation (tension gashes). Near self-juxtaposing faults a cleavage is developed sub-parallel to the fault plane, which combined with slickenfibers on competent bedding planes suggests bed-parallel slip.

Table 1: Self Juxtaposed Fault characteristics by lithology.

4.2.2 Faults that juxtapose multiple lithologies

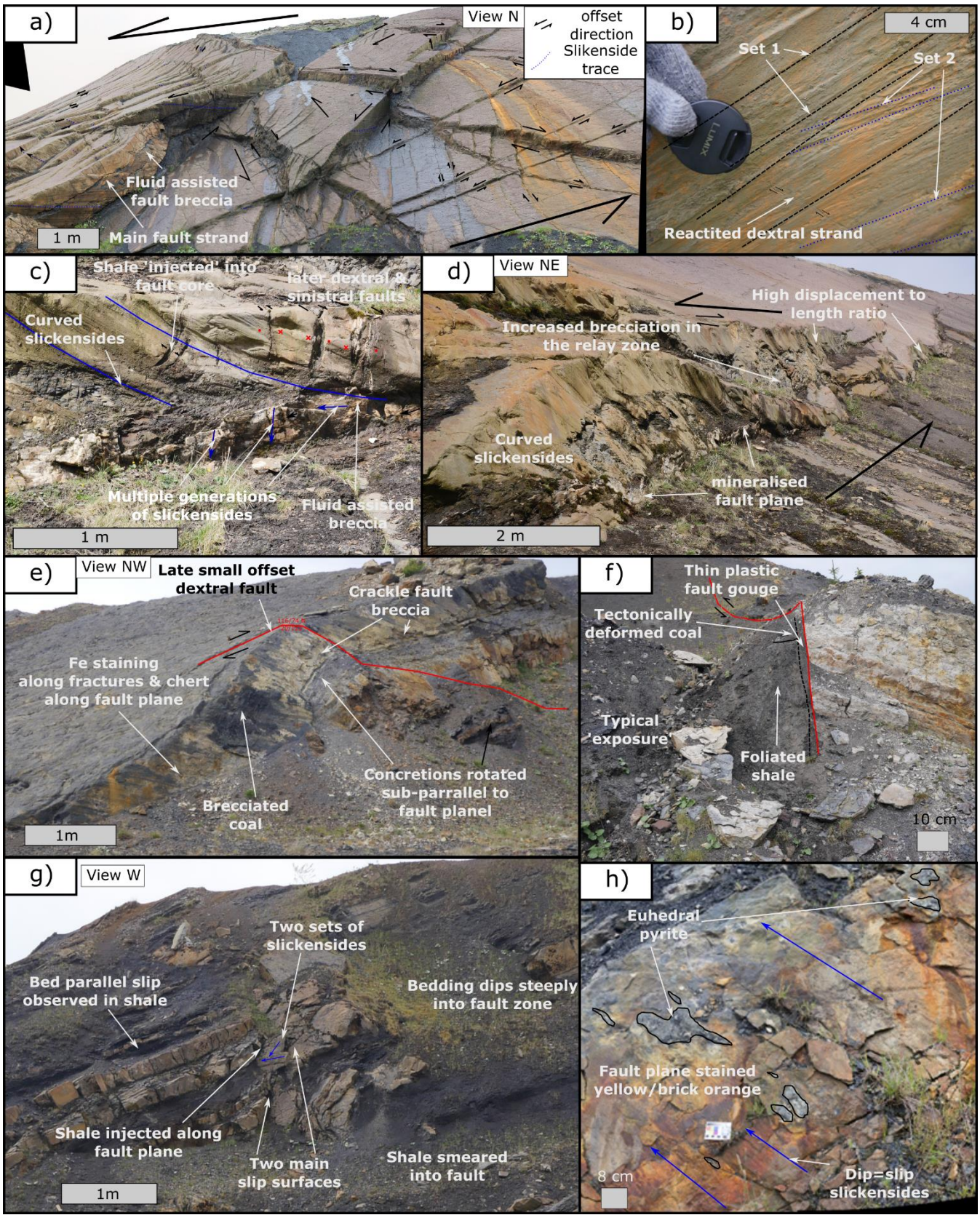

Figure 6: Characteristics of faults that cut multiple lithologies: a) complex fault mesh (after Sibson, (1996)) consisting of multiple strands of sinistral and dextral strike-slip fault planes (stratigraphic separation marked with arrows) picked out by shallow striations and the offset of the McDonald Limestone bedding plane; b) field photograph of a ~3 m stratigraphic separation

fault strand within the complex fault mesh (a) which displays multiple generations of fault striations, with local dextral reactivation separating striations belonging to set 2; c) fault architecture and d) view along a ~50 m strike-length of a highly segmented fault zone displaying 3 to 5 m stratigraphic separation exposed along the southerly dipping bedding dip-slope; fault architecture of the same 5 m stratigraphic separation fault cutting e) lithologies surrounding the McDonald Seat Earth, and g) interbedded sandstones, siltstones and shales of the Lower Limestone Coal Formation; f) primary slip plane of the ~80 m stratigraphic separation fault which cuts the west of the site; and h) shallowly dipping, sinistral dip-slip fault plane within a ~2 m thick sandstone bed of the Limestone Coal Formation.

Key features observed along faults that juxtapose multiple lithologies (i.e. that are not self-juxtaposing) are summarised in Table 2. Based on cross-cutting relationships we observe two phases of faulting at Spireslack SCM.

Larger stratigraphic offset (>5 m) faults that cut multiple lithologies display complex deformation styles (Figure 6, 7; Table 2) that depend on: a) the lithologies cut by the fault; b) the plane of observation (i.e. map (Figure 4) vs high wall (Figure 7)); and the phase of faulting (Figures 4, 5 & 6). Fault dips vary considerably between different lithologies, with steeper dips observed in competent lithologies (Figure 4d), as well as varying down dip along a single fault plane (Figure 6e, g; Table 2). Variations in fault dip causes bed rotation and the development of fault-core lenses consisting of sandstone and seat earth that are elongated parallel to fault strike lenses (Figure 4a, 6). Bedding is folded towards the faults (Figure 4 & 6), with folding more intense in interbedded lithologies (Figure 6g, 7) and shale (Figure 6f). The majority of throw on faults with over 5 m stratigraphic separation is accommodated along one (Figures 6b, c & 7a) or two (Fig. 7b) principal slip zones. Principal slip zones, particularly for Phase 1 faults, are typically straight and steep (>70°) (Figures 6 & 7) and are surrounded by a variably thick damage zone of shear fractures and self-juxtaposing faults (Figure 7), with thickness that varies between lithologies.

Fault core thickness is typically low (<5 cm) and displays a highly variable internal structure both along strike and down dip (Table 2, Figure 7). All faults display strike-parallel corrugations (Figure 6d, e, h) that often display brecciated coal (Figure 6e). Phase 1 faults are often mineralised with calcite (Figure 6c), display multiple slip events (Figure 6c), and locally display evidence of shale injected along the fault plane (Table 2). Conversely, Phase 2 faults rarely display calcite mineralisation and instead show evidence of syn-tectonic pyrite mineralisation (Figure 6h). Where Phase 1 and 2 faults interact, for example in the centre of the void (Figure 4a), a complex fault mesh is developed with displacement distributed over several sinistral and dextral fault strands (Figures 3 & 6a, b).

Fault (fault phase)	Stratigraphic separation	Lithologies cut	Fig(s)	Key Features
Fault meshes in the McDonald Lst. and LLF (Phase 1 & 2)	<3 m	Limestone, shale, locally siltstone	6a, 6b	• Bedding strongly rotated and tension gashes developed. • Fault cores are mineralized and thin (<5 cm) across all displacements. • Slickenfibers are curved and record multiple generations of fault slip.
Mineralised sinistral fault cutting the McDonald Lst	3 to 5 m	Limestone, shale	6c, 6d	• Fault planes mineralized and several have high displacement to length ratios. • Slickenfibers are curved and record multiple generations of fault slip. • Fluid assisted breccia, particularly in relay zones. • Phase 1 faults cut by Phase 2 faults. • Shale injected into fault core.
Dip-slip faulting of sandstones and seat earths (Phase 2)	3 to 5 m	Decimeter bedded seat-earth, sandstones and shale.	6h	• Shallowly dipping fault plane with dip-slip lineations. • Fault plane displays alteration and syn-kinematic euhedral pyrite. • Brecciated and friable coal present in the fault core.
Fault cutting interbedded lithologies. (Phase 1)	~5 m	Limestones, sandstones, seat-earth.	6b, 6c	• In seat earth fault dip changes from ~60° near the base of the outcrop to 79° near the top. • Brecciated coal is found within undulations on the fault plane. • Bedding in both Fig. 6b and 6c displays folding with wavelength decreasing and dip increasing towards the fault. • In the LLF a 2 to 3 m thick, mineralized fault zone is developed that displays multiple slip events. • Shale appears to have been locally injected into mineralized fractures.
Large fault cutting the whole sequence (Phase 1)	80 to 100 m	Interbedded lithologies of the LCF and LLF	6e	• Footwall damage zone consists of a highly fractured seat earth, with highly folded shale and altered coal in the hanging wall. • The fault core consists of a thin (<5 cm) fault gouge containing clasts of sandstone and organic fragments.
High wall, faults (Phase 1)	Fig 7a = 10 to 12 m Fig 7b = 6 to 10 m	Interbedded lithologies of the LCF and Spireslack Sandstone	7a, 7b	• The majority of throw is taken up by a small number of steep fault strands. • Fault-core thickness is typically thin (<5 cm) and highly variable down dip. • Fault-core lenses locally developed, particularly in interbedded units. • Damage zones vary in thickness depending on lithology and consist of an interconnected network of self-juxtaposing faults and shear fractures.

Table 2: Summary of the key features observed along faults that juxtapose multiple lithologies. Please see S3 for full field descriptions. LLF = Lower Limestone Formation, LCF = Limestone Coal Formation.

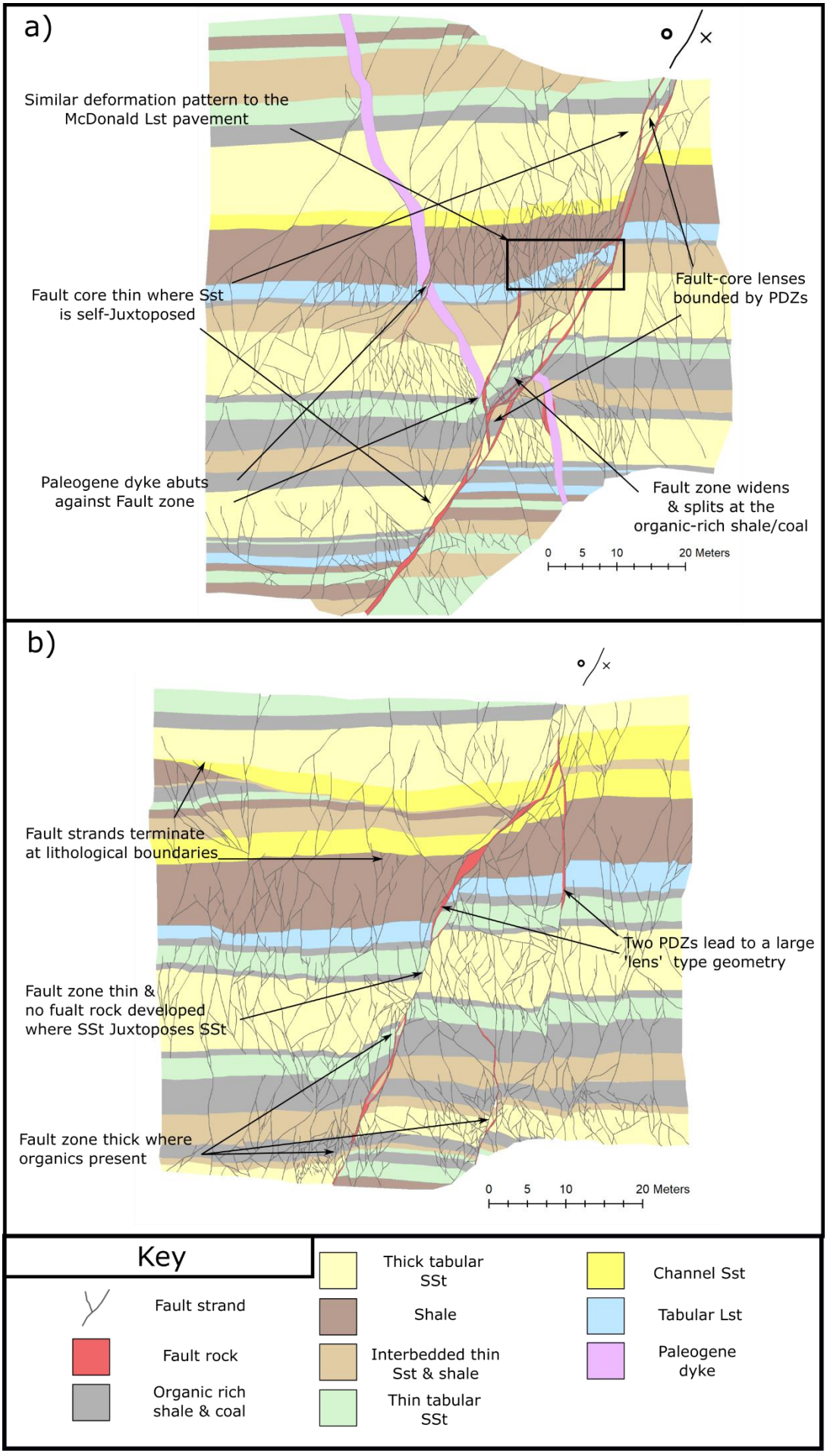
a)
Similar deformation pattern to the McDonald Lst pavement
Fault core thin where Sst is self-Juxtoposed
Paleogene dyke abuts against Fault zone
Fault-core lenses bounded by PDZs
Fault zone widens & splits at the organic-rich shale/coal
0 5 10 20 Meters
b)
Fault strands terminate at lithological boundaries
Two PDZs lead to a large 'lens' type geometry
Fault zone thin & no fualt rock developed where SSt Juxtoposes SSt
Fault zone thick where organics present
0 5 10 20 Meters
Key
Fault strand
Fault rock
Organic rich shale & coal
Thick tabular SSt
Shale
Interbedded thin Sst & shale
Thin tabular SSt
Channel Sst
Tabular Lst
Paleogene dyke

363

Figure 7: Digitised fault strands of sinistral faults cutting the Limestone Coal Formation exposed along the high wall: a) sinistral fault which displays between 2 and 5 m of apparent (vertical) throw. A later Paleogene dyke, associated with the British Tertiary Igneous Provence, intrudes across the fault, however, no evidence of white trap or dyke material is observed in the fault core [See table 4 for discussion]; b) sinistral fault with displays between 2 and 8 m apparent (vertical) throw along two principle displacement zones (PDZs). SSt = sandstone, Lst = Limestone. Photomontage provided courtesy of the British Geological Survey (BGS).

4.2.3 Interaction between faults and fractures within the McDonald Limestone

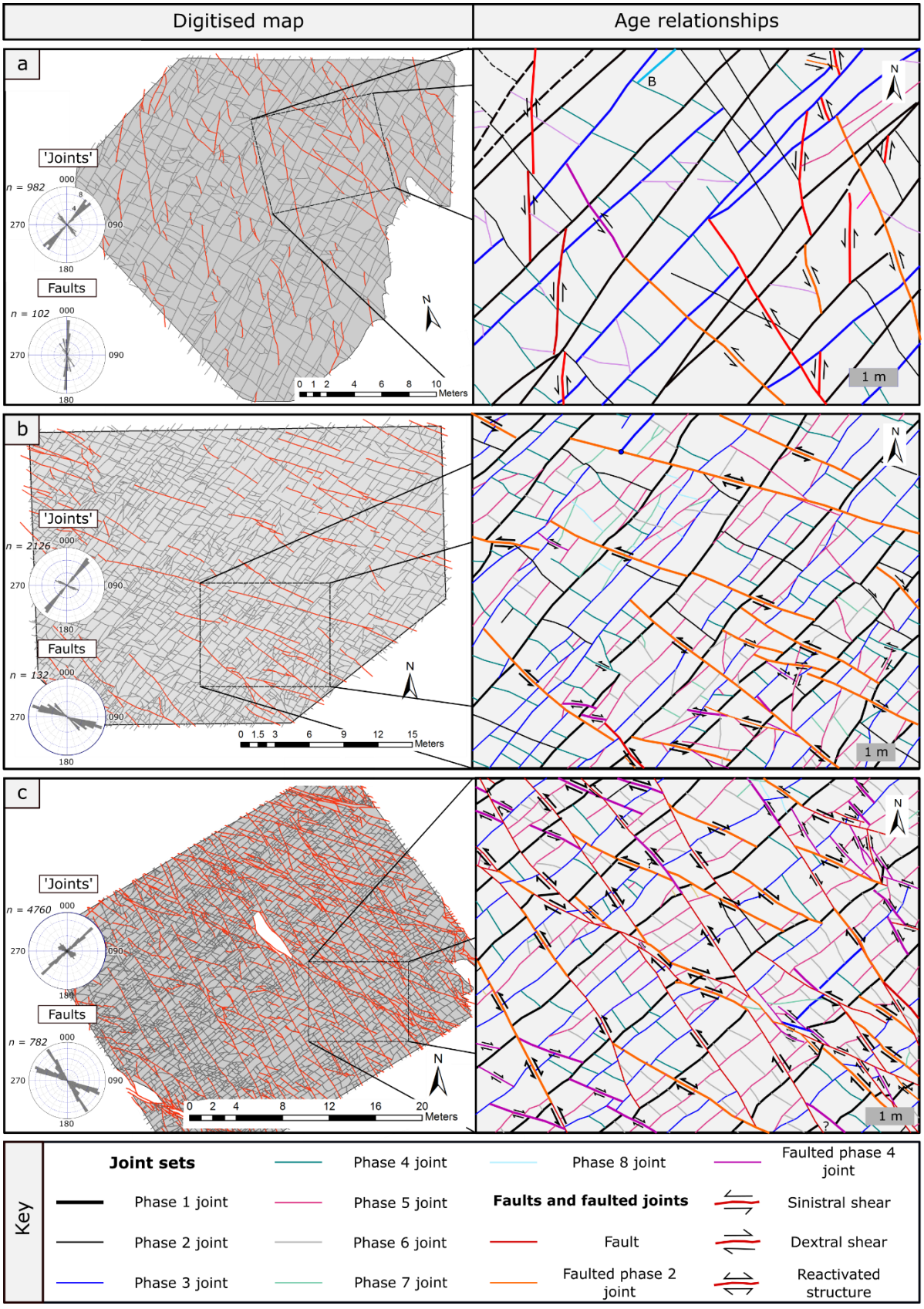

Figure 8 Fracture maps with increasing intensity of faulting: For each digitised map the exported fault (red lines) and 'joint' (dark grey lines) maps, along with the interpretation areas used for the

analysis (light grey) are provided. Please note that while it is possible some joint's and/or faults acted as trailing segments (cf. Nixon et al., 2014) no direct field evidence was observed.

The style of the fault and fracture network in the McDonald Limestone changes across the site (Figure 8) with the chronology and network properties of each sample area described below. In this section mineralised shear fractures, which are often faulted joints, are classified as faults for the network analysis.

Fracture relationships at low fault intensity:

The interpretation area in Figure 8a is dominated by large trace-length, NE trending, joints and smaller trace length NNW trending joints. Abutting relationships suggest these formed as four distinct phases, with two phases occurring at each orientation. The fault network displays two orientation sets (N and NNW) of sinistral faults with low connectivity, trace length, and intensity (Table 3). Both fault sets abut against favourably orientated Phase 1 or Phase 3 joints, indicating they formed later. Abutting relationships of Phase 3 joints against NNW trending faults suggesting Phase 2 joints were reactivated as faulted joints (after Zhao and Johnson, 1992) during the first phase of faulting. Phase 5 and 6 joints, that display variable orientations in Figure 8a, abut against the faults suggesting they formed later.

Fracture relationships where joints are favourably orientated for reactivation:

The interpretation area in Figure 8b, which is located slightly closer to the NW trending dextral fault zone that cuts the middle of the site (Figure 4), displays a similar intensity of faulting (I = 0.5 f/m), however, joint intensity is higher (I = 2.8 f/m). Joints from Phases 1 to 4 are observed in this panel; however, faulting caused the segmentation of NNW trending Phase 1 and 3 joints such that the recorded trace length of these joints in this panel is decreased compared to Figure 8a. Unlike Figure 8a, where only sinistral faults were observed, both sinistral and dextral offsets are present in Figure 8b. Fault orientations were typically either ENE or NE with the number of northerly faults significantly decreased (Table 3). Abutting relationships of faults in this panel suggests that the majority of strands represent reactivated Phase 2 (orange) or Phase 4 (purple) joints. The majority of faulted Phase 2 joints display sinistral offset or evidence of reactivation, while Phase 4 joints display predominantly dextral offsets. Abutting relationships suggest that faulting occurred as two phases, with joint development occurring both between (Phase 5 and 6) and following (Phase 7 and 8) the formation of dextral faults.

Fracture relationships where both phases of faulting is present

The interpretation area in Figure 8c is located close to the major NW-trending dextral fault (Figure 4), and includes two self-juxtaposing faults towards the bottom and top of the studied section (Figure 8c). The panel displays a complex fracture evolution, however, many of the features observed in the

previous panels are visible. Phase 1 to 4 joints are still easily identified; however, their trace length has further decreased due to increased fault intensity (I = 1.9 f/m). Unlike figures 8a and 8b, the fault network is well connected in this panel (Pc = 0.71), with individual fault strands linking to form locally complex relay zones (e.g. the bottom left of Figure 8c). Abundant sinistral, dextral, and reactivated fault strands are observed, with Phase 2 and 4 joints regularly becoming reactivated and linked by new fault strands. Locally, Phase 6 joints are also reactivated in a dextral sense (e.g., the relay zone in the NE of Figure 8c). The number of joints that abut against faults and the pre-existing joint sets (Phase 1 to 4) is greatly increased in this panel, with several Phase 7 and 8 joints identified.

Summary of structures

As fault intensity increases, the complexity of age relationships in the fault-fracture network also increases (Figure 8). Phase 1 to 4 joints are identified across all three panels and are interpreted as the 'pre-existing' joint network. As fault intensity increases, these 'pre-existing' features become segmented through faulting and their recorded trace length decreases. While fault intensity is similar in Figure 8a and 8b, faults with a N-S strike are only present in Fig 8a. This is probably due to the subtle anticlockwise rotation of the pre-existing joints relative to the stress field that enabled the reactivation of Phase 2 and 4 as faulted joints (Figure 8b, c) and promoted the formation of Phase 5 and 6 joints (orange and purple lines in Figure 8). The number of faulted joints drastically increases with increased fault intensity, with joints becoming linked through the formation of new fault strands. In agreement with the void-scale mapping (Figure 4), two phases of faulting have been identified in Figure 8b and 8c, with an earlier sinistral and later dextral phase. The sinistral phase appears to preferentially reactivate Phase 2 joints whereas the dextral phase preferentially reactivated both Phase 2 and 4 joints. The increase in reactivated joints, and two clear phases of faulting in Figure 8c explains the large increase in joint intensity in this panel (I = 4 f/m compared to I = 2.6 f/m in Figure 8a). While age relationships are reasonably consistent across this section of the limestone pavement, as fault-meshes begin to form, age relationships become increasingly complex and spatially variable (Figure 6a). This may be due to the development of 'trailing segments' (i.e. sections of a previous structure reactivated during subsequent deformation (c.f. Nixon et al., 2014)), however, no direct field evidence was observed as part of this study (e.g. mineralisation and/or evidence of shear). This suggests deformation occurred in a highly heterogeneous stress field, which was rotated relative to locally active fault strands. An increase in fault throw also affects the intensity, trace-length and connectivity of the network.

Sample area	Key features		# nodes				Pc	Orientation	# fr	Tl (m)			I (f/m)
			I	Y	X	E				Min	Max	Med.	
1 Fig. 8a	Faults are mineralized and display syntaxial crack seal growth textures.	'Joint'	212 (14%)	1028 (68%)	274 (18%)	6	0.95	0	132	0.09	14.71	4.02	1.3
								1	72	0.10	9.80	1.02	0.2
								2	400	0.12	7.33	0.89	1.0
								3	78	0.10	3.45	0.56	0.1
		Faults	169 (90%)	18 (10%)	0 (0%)	17	0.24	0	1	3.82	3.82	3.82	-
								1	0	-	-	-	-
								2	15	0.73	7.44	1.37	0.1
								3	86	0.22	9.33	1.62	0.4
2 Fig. 8b	SA2 is dominated by barren joints and shear fractures, with faults reactivating favorably orientated pre-existing joints.	'Joints'	1082 (25%)	2985 (68%)	297 (7%)	177	0.90	0	789	0.02	10.33	1.32	1.7
								1	174	0.10	4.18	0.70	0.2
								2	636	0.09	6.93	0.79	0.7
								3	454	0.09	4.44	0.59	0.4
								4	205	0.09	4.14	0.59	0.2
		Faults	264 (89%)	34 (11%	0 (0%)	34	0.28	0	-	-	-	-	-
								1	3	0.90	1.38	1.16	0.0
								2	24	0.47	13.16	2.43	0.3
								3	53	0.78	8.66	2.53	0.2
								4	19	0.21	3.16	1.74	0.0
3 Fig. 8c	The fault and fracture network is highly variable in SA3, with complex relationships between pre-existing joints, faulted joints, faults, and fracture corridors.	'Joints'	4517 (47%)	4726 (50%)	291 (3%)	234	0.77	0	2000	0.04	5.49	0.74	2.4
								1	464	0.06	2.97	0.39	0.3
								2	903	0.05	2.86	0.38	0.5
								3	1056	0.05	3.09	0.35	0.6
								4	355	0.05	1.90	0.28	0.2
		Faults	729 (55%)	593 (45%)	6 (0%)	172	0.71	0	7	0.35	2.81	0.95	0.0
								1	45	0.30	6.68	1.09	0.1
								2	341	0.10	9.38	1.42	0.8
								3	296	0.19	15.33	1.40	0.8
								4	93	0.21	8.15	1.11	0.2

Table 3 Network characteristics of the joint and fault datasets presented for the three sample areas outlined in Figure 8. Please note, because the fault network is superimposed onto the joint network, i-nodes (i.e. where a fault terminates) can represent a y-node in the combined network. Similarly, where a joint terminated against a fault, due to the sealing properties of the fault, it is no longer appropriate to classify this as a connected branch and as such is classified as an i-node in the 'joint network'. The percentage of each node classification is provided in brackets following the number of node counts. Trace length data is presented as orientation sets, that were derived following visual assessment of length weighted rose diagrams, and do not relate to the age sets outlined in Figure 8. For the combined network fracture statistics, and trace length distributions for all datasets please refer to S2.

5. Structural Evolution at Spireslack SCM

The exceptional 3D exposures of the Limestone Coal Formation and surrounding lithologies have informed a 5-stage conceptual model for the development of the structures (Table 4). While this model

is based on observations from Spireslack SCM, the model could be improved by utilising data from nearby open cast sites (Leslie et al., 2016), legacy subsurface data as introduced in Ellen et al. (2016), and additional correlation with the larger scale structures observed in the Midland Valley of Scotland.

Timing	Stage/regional	Faulting and folding	The whole sequence	McDonald Limestone	Muirkirk 6' Coal
Stage 1: Initial sedimentation and burial	Extensional reactivation of Caledonian lineaments led to NE-SE[1,2] or EW[3] orientated back-arc extension and rapid rift development[1, 2].	Although deposition was influence by fault movement (e.g. Spireslack Sandstone[4]), no evidence of early (Dinantian) extensional faults, that are common across the Midland Valley[5,6], are observed at Spireslack SCM.	During the Carboniferous the Midland Valley was located close to the equator[7], with sedimentation dominated by a coal bearing fluvio-deltaic depositional system[8,9].	Occasional marine incursions, caused by eustatic and tectonics controls, led to the deposition of regionally extensive marine limestones (e.g. the McDonald Limestones)[10]. A series of barren, sparsely spaced joints formed (Phase 1 & 2 joints) (Fig. 5), prior to being slightly rotated prior to the formation of Phase 3 & 4 joints. Joint Phases 1-4 represent the pre-faulting fracture state (Fig. 5a).	Peat swamps, that formed on swampy delta tops[11], were converted to coal during the process of coalification[12]. This causes cleats to form, with cleat orientation suggesting a NS orientated maximum compressive stress[13].
Stage 1b: Formation of the Muirkirk syncline	Folding in Ayrshire is attributed to late Visean syn-depositional compression[2].	Bedding became folded towards the SE, with the early influence of sinistral wrench tectonics (stage 2) possibly causing some NS orientated folds to develop (Fig. 3c).	Bed-parallel shear in shale (Fig 4d) was associated with regional folding and probably continued into Stage 2.		Early ankerite mineralization of N-trending face cleats (Fig. 2d-f).
Stage 2: Sinistral transpresion	Sinistral transpression widely effected the Midland Valley during the mid-to-late Carboniferous[2, 14], with structures at Spireslack SCM having been previously attributed to this stage[15].	Formation of sinistral offset faults with shallow lineations (Fig 3c) was accompanied by associated minor dextral faulting (Phase 1; Fig 3a, c) and local fault-related folds (Fig 6). Faults typically display mineralization (Figs 2, 4 & 6), with evidence of multiple crack-seal events (Fig 2c, e) .	Because of multiple pre-existing joint sets and a well-developed mechanical stratigraphy, trace length of individual fault strands is low and strain is taken up by several small faults.	Joint sets 1 and 3 restricted the growth of Phase 1 faults and favorably orientated Phase 2 joints were reactivated. Calcite mineralization commonly observed (Figs 4, 6) with evidence of multiple crack seal events (Fig. 2c). Joint sets 5 and 6 formed between Phase 1 and Phase 2 faults (Fig. 5b, c).	Sinistral en-échelon vein arrays and minor mineralized (Ankerite) shear fractures form (Fig. 2d, f). Faulting lead to the development of coal breccia and calcite veining which either cut across or abut against pre-existing structures (Fig. 2d-f)
Stage 3: Dextral transpression	Reversal in the shear direction during the Upper Carboniferous led to a period of Dextral transpression[14, 16, 2].	NW trending dextral faults formed (Phase 2 faults) (Fig 3a, c), with associated reactivation of Phase 1 faults and pre-existing structures (Fig. 5). Phase 2 fault zones display syn-kinematic pyrite (Fig. 6h).	Fault-zones became well connected through the linkage of through-going faults (Fig 5c). Where Phase 1 and 2 faults interact, complex fault meshes developed (Fig 3a, 6a).	Joint sets 1 & 3 restricted the growth of Phase 2 faults, with joint sets 2, 4, and locally 6 being reactivated (Fig 5, b, c). Linking faults are preferentially orientated between 060° and 100° (Figs. 5c & 8) and joint sets 7 & 8 formed following Phase 2 faults (Fig 5b, c).	Reactivation of cleats and stage 2 features was accompanied by a further phase of ankerite mineralization, and local kink-band development (Fig 2 d-f).
Stage 4: Paleogene intrusions.	Basaltic dykes were intruded, with the orientation suggesting it is associated with the British Tertiary Igneous Provence[17].	No fragments of dyke are observed within the fault core in Fig 7a and no white trap is observed in the coal within the fault. This provides evidence that the tertiary dyke, that postdated faulting did not intrude along the fault plane. Instead, it is likely that the dyke either injected around the tip of the fault, or broke through the fault core out of the plane of observation.	Dyke orientation traced along the trend Phase 1 and 2 faults (Fig. 3).	In the high wall the Muirkirk 9' coal becomes altered to white trap in the vicinity of the dyke, a common trend in the Western Ayrshire Coalfield[18]. It is unclear whether the 6" coal has also been altered to white trap dur to the seam not being exposed.	

Stage 5: Post- Paleogene reactivation	**NW-SE and locally NE-SW trending structures were reactivated, possibly associated with isostatic rebound or the opening of the North or Irish Seas.**	**No evidence of extensional reactivation is observed other than along the edge of the dyke.**	**Brecciation of the edge of the major dyke and surrounding limestones was coupled with dip-slip reactivation, suggesting post-intrusion extensional reactivation occurred.**	**No evidence of late stage reactivation observed.**

Table 4: Summary of the structural features observed at Spireslack SCM. References in the table: 1) Leeder (1982); 2) Underhill et al. (2008); 3) Haszeldine (1984); 4) Ellen et al. (2019); 5) Coward, (1993); 6) Anderson (1951); 7) Soper et al. (1992); 8) Browne et al. (1999); 9) Read et al., (2002); 10) George, (1978); 11) Thomas (2013); 12) O'Keefe et al. (2013); 13) Rippon et al. (2006); 14) Ritchie et al. (2003); 15) Leslie et al., (2016); 16) Caldwell and Young (2013); 17) Emeleus and Gyopari (1992); 18) Mykura (1965).

6. Discussion

6.1 The effect pre-existing joints and coal cleats on subsequent deformation and network connectivity

The mechanically stratified succession at Spireslack SCM has led to the development of a fracture stratigraphy (Laubach et al., 2009). While joints across the site locally display two 'orientation sets' (Figure 8, insets), abutting relationships discussed in section 4.4.3 identified 8 'age sets' punctuated by two phases of faulted joints (Figure 8). Different 'orientation sets' have previously been attributed to separate tectonic events (e.g. Vitale et al., 2012), or situations where the intermediate ($\sigma 2$) and minimum ($\sigma 3$) principal stresses are nearly identical, and can therefore easily switch between each other (Caputo, 1995; Caputo and Hancock, 1998). It is likely the latter that contributes to the rapid switching between ~NNW (Phase 1, 3, 5, & 7) and ~NE (Phase 2, 4, 6, & 8) trending joint sets observed in Figure 8.

There are several examples of joints or cleats influencing fault growth at Spireslack SCM (Figure 3, 5, 8). Jones and Tanner (1995) found that transpressional strain can often become partitioned across pre-existing structures. At Spireslack, joints appear to be accommodating the shear-strain component, with pure-shear accommodated through the tightening of the Muirkirk Syncline. Throughout both deformation phases, faults abutted against NE trending joint sets. However, during the sinistral phase of faulting, larger trace length N to NNW trending cleats and joints (e.g. Phase 2 joints, Fig. 5a) were reactivated. As the principal stress orientation changed to enable the formation of phase 2 dextral faults (Figure 4c), faulted joints associated with the 1st phase of faulting became reactivated (Figure 8c), with Phase 4 joints preferentially reactivated (Figure 8b, c). Phase 2 joints only became reactivated in the vicinity of self-juxtaposing dextral faults (NW-SE trending feature cutting Figure 8c). The preferential reactivation of specific joint sets could be due to:

a) Changes in the mechanical properties of lithologies at Spireslack SCM due to mineralisation associated with Phase 1 faults. For example, coal cleats, that previously acted as a weakness in the rock (Li et al., 2016), act as strength inclusions following ankerite mineralisation, enabling barren shear fractures to develop (Figure 3d).
b) Subtle differences in joint orientation between sets (Figure 8, inset) changes the relative orientation of features to the stress field (e.g. Moir et al., (2010); Zhao and Johnson, (1992)), and alters the stress ratio across the fracture (Chang and Haimson, 2000; Haimson and Chang, 2000).
c) Differences in mechanical properties of the fracture surface. For example, due to their longer trace length, fracture roughness (Nasseri et al., 2009; Tsang and Witherspoon, 1983) could

492 increase in Phase 1 joints in comparison to smaller trace length Phase 3 or 5 joints (Reed et
493 al., 2008).

494 The fact that some joints show evidence of preferential reactivation and subsequent cementation, while
495 others remain barren, suggests that certain joint sets indicate the past-connectivity of mineral rich fluids
496 through the network, which at Spireslack SCM was dominated by faults (Figure 8). Barren joints
497 typically post-date mineralisation (Peacock, 2001; Peacock and Sanderson, 2018), however, Phase 1
498 and 3 joints at Spireslack are often offset by faults or reactivated as faulted joints (Figure 8). This
499 suggests joints were present at the time of faulting, however, not all joints sets were hydraulically
500 connected to the mineralising fluids. This could be either due to: fluid flow being dominated by vertical
501 flow associated with fault-valve behaviour during slip events (Sibson, 1990, 1992); micro-cataclasite
502 and/or mineralisation along joints that were not visible during field observations or had been weathered
503 out during subsequent groundwater flow; or mineralisation occurred under a stress-induced flow pattern
504 that had a relatively high stress ratio ($k < 3$). This would result in flow becoming channelised along
505 favourably orientated features while those sub-optimally orientated are not dilated and therefore contain
506 no, or very little, flow (Baghbanan and Jing, 2008).

507 Groundwater flow within Carboniferous aquifers is dominated by bed-parallel fracture flow
508 (Dochartaigh et al., 2015). While the combined fault-fracture network across the McDonald limestone
509 displays very high network connectivity (Pc = 0.99 to 1.00) and high fracture density (D = 3.1 to 5.9
510 f/m^2) (Figure 9, S2), mineralised faults (Figures 5, 6) may act as a baffle or barrier to flow (e.g.
511 (Skurtveit et al., 2015). It is therefore more appropriate to consider the 'joint network' when assessing
512 the modern-day network connectivity at the site. While joint intensity increases as fault-intensity
513 increases (Table 3) this is not the case for connectivity. Where faulting intensity was low, joints are well
514 connected (SA1, Pc = 0.95). However, as fault intensity increased and the number of faulted joints
515 increases (SA2), connectivity drops to Pc = 0.90. In SA3, where fault intensity is 1.9 f/m, the
516 connectivity of the joint network drops to Pc = 0.77. Additionally, connectivity depends on the
517 orientation of the fractures, with NW trending features being the most connected (Table 3, Figure 9c).
518 The modern day stress orientation in Scotland (roughly northerly trending maximum compressive stress
519 (Baptie, 2010; Heidbach et al., 2008)) would act to reduce the aperture of these large trace length joint
520 sets and further reduce the permeability of the network

521 The drop on connected joints is shown in the trends (pink arrows) on Figure 9 and is caused by the
522 gradual increase in abutting relationships between fault's and joints. As more joints become reactivated
523 as faults, the fault network becomes more connected as splays (i.e. y-nodes; Figure 8) develop, whilst
524 reducing the number of connected joints (i.e. x- and y- nodes in the 'joint' dataset) (Figure 8). Similarly,

as the intensity and connectivity of the fault network increases, the number of abutting relationships between joints and faults increases. The increases the number of i-nodes in the joint network and gradually decreases the number of connected branches as the intensity of faulting increases. This leads to the counter-intuitive observation that although joint intensity increases in areas associated with faulting (Table 3), the cementation of faults and faulted joints causes the connectivity of the modern day network in these areas to be lower (Figure 9).

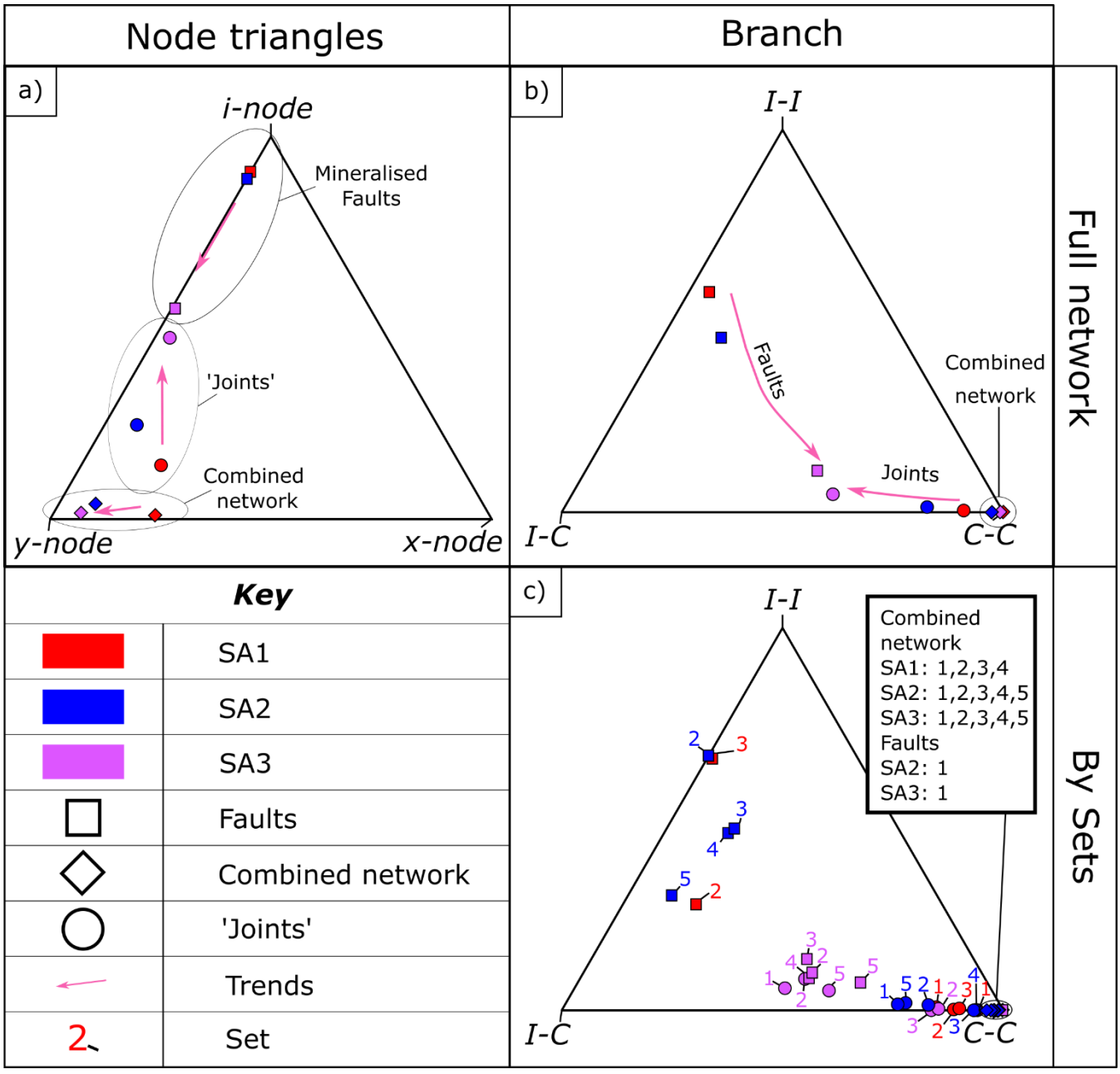

Figure 9: Network topology data. Node and branch triangle (after Sanderson & Nixon (2015)) for the joint, fault, and combined fracture networks for the three samples areas shown in Figure 8: a) node and b) branch data presented by sample area for the fault, joint, and combined networks, and c) branch data by sets, as outlined in S2, to investigate the directionality of network connectivity. Please see the main text for a description of the main trends.

6.2 The role of lithology on faulting style: the importance of lithological juxtaposition

The internal structure of faults at Spireslack SCM is greatly affected by the level of lithological juxtaposition, with different properties observed for self-juxtaposing faults (Section 4.2.1) and those that cut multiple lithologies (Section 4.2.2). Self-juxtaposing fault-strands cutting lithologies without pre-existing joints are typically relatively planar, develop relay zones, and only display local iron staining along fault planes (e.g. the 6' seat earth; Figure 5a, b). Conversely, in lithologies where pre-existing weaknesses influence the growth of faults, multiple sets of lineations on fault planes and the presence of compound veins provide evidence for multiple slip events (McDonald Limestone; Figure 3a, c, 6b & 8). This suggests that faults in these lithologies initiated as a segmented fault-fracture mesh (Sibson, 1996), with field evidence suggesting mineralising fluid flow in the McDonald limestone and coal occurred as multiple crack-seal events (Figure 3c, e). This implies that self-juxtaposing faults cutting the McDonald limestone and 6' coal at Spireslack behaved in a similar manner to other faults in carbonates with fluid pathways only remaining open for a small amount of time and probably closing following fault slip (c.f Billi et al. 2003; Sibson, 1990, 1992). Mineralised Phase 1 faults that cut multiple lithologies also display multiple slip events (Figure 6c) and matrix (calcite) supported fault breccias located within relay zones (Figure 6d), intersections between Phase 1 and 2 faults (Figure 6c), and at asperities along the principle slip zone (Figure 6a). This suggests fault valve behaviour was also present along non-self-juxtaposing faults (Peacock et al., 2019; Sibson, 1990).

Where faults cut multiple lithologies, shale accommodates the rotation of bedding, leading to rotated blocks and multiple generations of curved slickensides (Figure 6). As shale is buried and compressive stresses increase, the ratio of pre-consolidation stress and compaction-related stresses control the behaviour or shales and mud rocks (Yuan et al., 2017; Nygård et al., 2006). As a general rule, shales are ductile during burial, and brittle during exhumation where they experience stresses below the maximum stress they have encountered. Ductile behaviour of the shales at the time of faulting suggests that both phases of faulting occurred prior to maximum burial, which is estimated at <3,000 m at around 60 Ma for the Limestone Coal Formation (Monaghan, 2014).

Fault cores at Spireslack SCM also differ between self-juxtaposing faults (Figure 5) and those that cut multiple lithologies (Table 2). Wilkins *et al.* (2001), studying growth of normal faults through jointed lithologies, found similar observations to those at Spireslack SCM with little fault rock development (Figure 3a, 5f), and considerably smaller displacement/length ratios than that expected for faults which do not cut jointed lithologies (Figure 5f, 6a, d). While fault core at Spireslack SCM is typically thin (Table 2), similar to previous studies (e.g. McKay et al., 2019; De Rosa et al., 2018) thickness was found to be highly heterogeneous both along strike and down dip. Much of this variability is caused by

570 the lithological juxtapositions observed across the fault (Figure 7), asperities on the principal slip zone
571 (Figure 6), the degree of folding (Figure 6) and the presence of fault core lenses (Figure 7). In
572 agreement with the fault growth model of Childs et al. (2009), the highly segmented network of self-
573 juxtaposing faults (Figure 8), and differences in fault dip between lithologies (Figure 4d), contribute to
574 the heterogeneity observed in the fault-cores of faults that cut multiple lithologies.

575 Our data demonstrates that the evolution of faults and fault zone structure, and therefore the bulk
576 hydraulic properties of the rock mass at Spireslack SCM, varied both through time and as faults cut
577 multiple lithologies. The abundance of faults within competent lithologies that cannot be traced into
578 shale interbeds suggests faults at Spireslack SCM initiated as segmented fault strands within competent
579 lithologies (e.g. limestones) and the coals (Figures 5, 8), with shale interbeds. They restricted fault
580 growth and instead accommodating ductile deformation. Despite faulting being dominantly strike slip,
581 the oblique orientation of faults to bedding across the site meant that many fault-growth models derived
582 from observations and modelling of normal faults in mechanically layered sequences appear to be valid
583 (e.g. (Childs et al., 1996; Ferrill et al., 2017; Schöpfer et al., 2006, 2007, 2016) . However, it is also
584 clear that the initial segmented fault network within the competent layers was strongly controlled by the
585 presence and evolution of the joints and mineralised fault zones (Figure 8). It is therefore helpful to
586 consider the concept of lithological juxtaposition, the presence and behaviours of shale interbeds, and
587 the relative timing of deformation, when considering the growth and internal structure of fault growth in
588 mechanically layered sequences.

6. Conclusions

The exceptional exposures of the Limestone Coal Formation at Spireslack SCM provides an excellent opportunity to examine the role of lithology and pre-existing structures on fault evolution, internal structure and connectivity. Careful mapping to unpick cross-cutting relationships has revealed a 5 stage, complex geological evolution for the Spireslack SCM succession consisting of two phases of faulting and eight phases of joint development:

Stage 1: Pre-existing weaknesses developed in the fluvial deltaic sequences at Spireslack SCM as cleats and joints formed during burial of the fluvial-deltaic host rocks and formation of the regional Muirkirk syncline (***Stage 1b****).*

Stage 2: Sinistral transpression caused the formation of Phase 1 faults, with self-juxtaposing faults laterally restricted by NE trending cleats and Phase 1 and 3 joints. The same transpression preferentially reactivates Phase 2 joints to form faulted joints. Larger faults, which cut multiple lithologies, developed a complex mineralised fault core with multiple slip events.

Stage 3: Dextral transpression caused the formation of NW trending Phase 2 faults with self-juxtaposing faults restricted by pre-existing joints or cleats, and larger faults restricted by Phase 1 faults. Phase 2 faults led to the reactivation of Phase 3 joints and reactivated Phase 1 faulted joints. Where Phase 1 and Phase 2 faults interact, complex zones of deformation develop.

Stage 4: Paleogene igneous dykes cut across the site, preferentially exploiting Phase 2 faults, and display post intrusion extensional reactivation (***Stage 5).***

While the overall fracture density increases around the larger faults, counter-intuitively the modern day network connectivity decreases in these areas due to the cementation of faults and joints.

We find that the fault zone internal structure at Spireslack SCM depends on: a) whether the fault is self-juxtaposing or cuts multiple lithologies; b) the presence and ductility of shale layers, which in turns leads to bed-rotation and fault-core lens formation; and c) the orientation of open and mineralised joints/coal cleats at the time of faulting. Self-juxtaposing faults are strongly affected by the orientation, and mineralisation of pre-existing joint-sets and coal cleats, causing them to grow as multiple segmented fault strands within competent lithologies. Self-juxtaposing faults only become well connected where fault intensity is high. Faults that cut multiple lithologies are strongly affected by the presence of shale interbeds and display a complex and heterogenous fault structure with fault length limited by the presence of pre-existing faults. Therefore, it is crucial to appreciate the relative timing of deformation events, concurrent or subsequent cementation and the degree of lithological juxtaposition when considering the mechanical and hydraulic properties of a mechanically stratified succession.

Acknowledgements

This work was funded through BJA's PhD studentship, supported by the Environmental and Physical Sciences Research Council (EPSRC, award number EP/L016680/1). LMcK is supported by a University of Strathclyde Environmental and Physical Science Research Council (EPSRC) Doctoral Training Partnership (DTP) award (award reference 1904102). We would like to thank Dave Healy for the use of the high-resolution photomontage of the McDonald Limestone dip slope and the British Geological Society for the use of the photomontage of the high wall.

References

Anderson, E. M.: The dynamics of faulting and dyke formation with applications to Britian, Oliver & Boyd, Edinburgh., 1951.

Andrews, B. J., Roberts, J. J., Shipton, Z. K., Bigi, S., Tartarello, M. C. and Johnson, G. O.: How do we see fractures? Quantifying subjective bias in fracture data collection, Solid Earth, 10(2), 487–516, doi:https://doi.org/10.5194/se-10-487-2019, 2019.

Baghbanan, A. and Jing, L.: Stress effects on permeability in a fractured rock mass with correlated fracture length and aperture, Int. J. Rock Mech. Min. Sci., 45(8), 1320–1334, doi:https://doi.org/10.1016/j.ijrmms.2008.01.015, 2008.

Baptie, B.: Seismogenesis and state of stress in the UK, Tectonophysics, 482(1–4), 150–159, doi:10.1016/j.tecto.2009.10.006, 2010.

Bluck, B. J.: Pre-Carboniferous history of the Midland Valley of Scotland, Trans. R. Soc. Edinb. Earth Sci., 75(2), 275–295, doi:10.1017/S0263593300013900, 1984.

Bons, P. D., Elburgm, M. . and Gomez-Rivas, E.: A review of the formation of tectonic veins and their microstructures, J. Struct. Geol., 43, 33–62, doi:https://doi.org/10.1016/j.jsg.2012.07.005, 2012.

Browne, M. A. E. and Monro, S. K.: Evolution of the coal basins of Central Scotland, in Congrès International de Stratigraphie et de Géologie du Carbonifère, pp. 1–19, Nanjing University Press, Nanjing, Beijing., 1987.

Browne, M. A. E., Dean, M. T., Hall, I. H. S., McAdam, A. D., Monro, S. K. and Chisholm, J. I.: A lithostratigraphical framework for the Carboniferous rocks of the Midland Valley of Scotland, Keyworth, Nottingham: British Geological Survey., 1999.

Caldwell, W. G. E. and Young, G. M.: The Cumbrae Islands: A structural Rosetta Stone in the western offshore Midland Valley of Scotland, Scottish J. Geol., 49(2), 117–132, doi:10.1144/sjg2011-462, 2013.

Caputo, R.: Evolution of orthogonal sets of coeval extension joints, Terra Nov., 7(5), 479–490, doi:10.1111/j.1365-3121.1995.tb00549.x, 1995.

Caputo, R. and Hancock, P. L.: Crack-jump mechanism and its implications for stress cyclicity during extension fracturing, J. Geodyn., 27(1), 45–60, doi:10.1016/S0264-3707(97)00029-X, 1998.

Chang, C. and Haimson, B.: True triaxial strength and deformability of the German Continental Deep Drilling Program (KTB) deep hole amphibolite, J. Geophys. Res. Solid Earth, 105(B8), 18999–19013, doi:10.1029/2000jb900184, 2000.

Childs, C., Nicol, A., Walsh, J. J. and Watterson, J.: Growth of vertically segmented normal faults, J. Struct. Geol., 18(12), 1389–1397, doi:10.1016/S0191-8141(96)00060-0, 1996.

Childs, C., Manzocchi, T., Walsh, J. J., Bonson, C. G., Nicol, A. and Schöpfer, M. P. J.: A geometric model of fault zone and fault rock thickness variations, J. Struct. Geol., 31(2), 117–127,

662 doi:10.1016/j.jsg.2008.08.009, 2009.

663 Coward, M. P.: The effect of Late Caledonian and Variscan continental escape tectonics on basement
664 structure, Paleozoic basin kinematics and subsequent Mesozoic basin development in NW Europe, in
665 Petroleum Geology Conference Proceedings, vol. 4, pp. 1095–1108, Geological Society of London.,
666 https://doi.org/10.1144/0041095, 1993.

667 Crider, J. G. and Peacock, D. C. P.: Initiation of brittle faults in the upper crust: A review of field
668 observations, J. Struct. Geol., 26(4), 691–707, doi:10.1016/j.jsg.2003.07.007, 2004.

669 Cruikshank, K. M., Zhao, G. and Johnson, A. M.: Analysis of minor fractures associated with joints and
670 faulted joints, Journal of Structural Geology, 13(8), 865-886, https://doi.org/10.1016/0191-
671 8141(91)90083-U, 1991.

672 Davis, A.: Carboniferous rocks of the Muirkirk, Gass Water and Glenmuir areas of Ayrshire, Bull Geol
673 Surv GB, 40, 1–49, 1972.

674 Dean, M. T., Browne, M. A. E., Waters, C. N. and Powell, J. H.: A lithostratigraphical framework for
675 the Carboniferous successions of northern Great Britain (onshore), Br. Geol. Surv. Res. Rep., RR/10/07,
676 174, 2011.

677 Dershowitz, W. S. and Einstein, H. .: Characterizing Rock Joint Geometry with Joint System Models,
678 Rock Mech. Rock Eng., 21(1), 21–51, https://doi.org/10.1007/BF01019674, 1988.

679 Dochartaigh, B. É. Ó., Macdonald, A. M., Fitzsimons, V. and Ward, R.: Scotland's aquifers and
680 groundwater bodies, Br. Geol. Surv. Res. Rep., OR/15/028, 63 [online] Available from:
681 www.bgs.ac.uk/gsni/ (Accessed 11 October 2019), 2015.

682 Donath, F. A.: Experimental study of shear failure in anisotropic rocks, Geol. Soc. Am. Bull., 72, 985–
683 990, doi:https://doi.org/10.1130/0016-7606(1961)72[985:ESOSFI]2.0.CO;2, 1961.

684 Donnelly, L. J.: A review of coal mining induced fault reactivation in Great Britain, Q. J. Eng. Geol.
685 Hydrogeol., 39, 5–50, DOI: 10.1144/1470-9236/05-015, 2006.

686 Dunham, K.C.: Geology of the Northern Pennine Orefield Volume 1 Tyne to Stainmore. HMSO,
687 London, UK, 1948.

688 Ellen, R., Callaghan, E., Leslie, A. G. and Browne, M. A. E.: The rocks of Spireslack surface coal mine
689 and its subsurface data: an introduction, Br. Geol. Surv. Res. Rep., OR/16/053, 38, 2016.

690 Ellen, R., Browne, M. A. ., Mitten, A. ., Clarke, S. M., Leslie, A. G. and Callaghan, E.: Sedimentology,
691 architecture and depositional setting of the fluvial Spireslack Sandstone of the Midland Valley,
692 Scotland: insights from the Spireslack surface coal mine, Geol. Soc. London, Spec. Publ., 488, SP488-2,
693 https://doi.org/10.1144/SP488.2, 2019.

694 Emeleus, C. H. and Gyopari, M. C.: British Tertiary Igneous Province, Chapman and Hall, London,
695 UK., 1992.

Ferrill, D. a. and Morris, A. P.: Dilational normal faults, J. Struct. Geol., 25, 183–196, doi:10.1016/S0191-8141(02)00196-7, 2003.

Ferrill, D. A. and Morris, A. P.: Fault zone deformation controlled by carbonate mechanical stratigraphy, Balcones fault system, Texas, Am. Assoc. Pet. Geol. Bull., 92(3), 359–380, doi:10.1306/10290707066, 2008.

Ferrill, D. A., McGinnis, R. N., Morris, A. P. and Smart, K. J.: Hybrid failure: Field evidence and influence on fault refraction, J. Struct. Geol., 42, 140–150, doi:10.1016/j.jsg.2012.05.012, 2012.

Ferrill, D. A., Morris, A. P., McGinnis, R. N., Smart, K. J., Wigginton, S. S. and Hill, N. J.: Mechanical stratigraphy and normal faulting, J. Struct. Geol., 94, 275–302, doi:10.1016/j.jsg.2016.11.010, 2017.

Francis, E. H.: Carboniferous: in CRAIG, in The Geology of Scotland, pp. 253–296, Scottish Academic Press, Edinburgh., 1991.

George, T. N.: Eustasy and tectonics: Sedimentary rhythms and stratigraphical units in British Dinantian correlation, in Proceedings of the Yorkshire Geological Society, vol. 42, pp. 229–262, https://doi.org/10.1144/pygs.42.2.229, 1978.

Gibson, R. G. and Bentham, P. A.: Use of fault-seal analysis in understanding petroleum migration in a complexly faulted anticlinal trap, Columbus Basin, offshore Trinidad, Am. Assoc. Pet. Geol. Bull., 87(3), 465–478, doi:10.1306/08010201132, 2003.

Haimson, B. and Chang, C.: A new true triaxial cell for testing mechanical properties of rock, and its use to determine rock strength and deformability of Westerly granite, in International Journal of Rock Mechanics and Mining Sciences, vol. 37, pp. 285–296, https://doi.org/10.1016/S1365-1609(99)00106-9, 2000.

Haszeldine, R. S.: Carboniferous North Atlantic palaeogeography: Stratigraphic evidence for rifting, not megashear or subduction, Geol. Mag., 121(5), 443–463, doi:10.1017/S0016756800029988, 1984.

Healy, D., Jones, R. R. and Holdsworth, R. E.: Three-dimensional brittle shear fracturing by tensile crack interaction, Nature, 439(7072), 64–67, doi:10.1038/nature04346, 2006.

Heidbach, O., Tingay, M., Barth, A., Reinecher, J., Kurfeß, D. and Müller, B.: The world stress map database release, WSM, Rel2008(9) [online] Available from: doi: 10.1594/GFZ, 2008.

Holland, M. and Urai, J. L.: Evolution of anastomosing crack–seal vein networks in limestones: Insight from an exhumed high-pressure cell, Jabal Shams, Oman Mountains, J. Struct. Geol., 32(9), 1279–1290, doi:https://doi.org/10.1016/j.jsg.2009.04.011, 2010.

Jones, R. . and Tanner, P. W. G.: Strain partitioning in transpression zones, J. Struct. Geol., 17(6), 793–802, doi:https://doi.org/10.1016/0191-8141(94)00102-6, 1995.

Kattenhorn, S. A., Aydin, A. and Pollard, D. D.: Joints at high angles to normal fault strike: An explanation using 3-D numerical models of fault-perturbed stress fields, J. Struct. Geol., 22(1), 1–23, doi:10.1016/S0191-8141(99)00130-3, 2000.

731 Knai, T. A. and Knipe, R. J.: The impact of faults on fluid flow in the Heidrun Field, Geol. Soc. Spec.
732 Publ., 147(1), 269–282, doi:10.1144/GSL.SP.1998.147.01.18, 1998.

733 Lăpădat, A., Imber, J., Yielding, G., Iacopini, D., McCaffrey, K. J. W., Long, J. J. and Jones, R. R.:
734 Occurrence and development of folding related to normal faulting within a mechanically heterogeneous
735 sedimentary sequence: A case study from Inner Moray Firth, UK, Geological Society Special
736 Publication, vol. 439, pp. 373–394, https://doi.org/10.1144/SP439.18, 2017.

737 Laubach, S. E., Marrett, R. A., Olson, I. E. and Scott, A. R.: Characteristics and origins of coal cleat: a
738 review, Int. J. Coal Geol., 35(1–4), 175–207, doi:10.1016/S0166-5162(97)00012-8, 1998.

739 Laubach, S. E., Olson, J. E. and Cross, M. R.: Mechanical and fracture stratigraphy, Am. Assoc. Pet.
740 Geol. Bull., 93(11), 1413–1426, doi:10.1306/07270909094, 2009.

741 Leeder, M. R.: Upper Palaeozoic basins of the British Isles-Caledonide inheritance versus Hercynian
742 plate margin processes, J. Geol. Soc. London, 139(1980), 479–491, doi:10.1144/gsjgs.139.4.0479,
743 1982.

744 Leeder, M. R.: Recent developments in Carboniferous geology: a critical review with implications for
745 the British Isles and N.W. Europe, Proc. Geol. Assoc., 99(2), 79–100, https://doi.org/10.1016/S0016-
746 7878(88)80001-4, 1988.

747 Leslie, A. G., Browne, M. A. E., Cain, T. and Ellen, R.: From threat to future asset—The legacy of
748 opencast surface-mined coal in Scotland, Int. J. Coal Geol., 164, 123–133,
749 doi:10.1016/j.coal.2016.06.017, 2016.

750 Li, Y. W., Zhang, J. and Liu, Y.: Effects of loading direction on failure load test results for Brazilian
751 tests on coal rock, Rock Mech. Rock Eng., 49(6), 2173–2180, doi:10.1007/s00603-015-0841-8, 2016.

752 Long, J. J. and Imber, J.: Geological controls on fault relay zone scaling, J. Struct. Geol., 33(12), 1790–
753 1800, doi:10.1016/j.jsg.2011.09.011, 2011.

754 Lunn, R.J., Willson, J.P., Shipton, Z.K. and Moir, H.:Simulating brittle fault growth from linkage of
755 preexisting structures, Journal of Geophysical Research: Solid Earth, 113(B7),
756 **https://doi.org/10.1029/2007JB005388**, 2008.

757 Manzocchi, T.: The connectivity of two-dimensional networks of spatially correlated fractures, Water
758 Resour. Res., 38(9), 1-1-1–20, doi:10.1029/2000WR000180, 2002.

759 McKay, L., Shipton, Z. K., Lunn, R. J., Andrews, B. J., Raub, T. and Boyce, A. J.: Detailed Internal
760 Structure and Along-Strike Variability of the Core of a Plate Boundary Fault: The Highland Boundary
761 Fault, Scotland, J. Geol. Soc. London., doi:https://doi.org/10.1144/jgs2018-226, 2019.

762 Microsoft: “Glenbuck, Aryshire” [1:2,000] (Map). Bing Maps., Aer. Photogr. [online] Available from:
763 https://www.bing.com/maps/, 2017.

764 Moir, H.: Modelling fault zone evolution : the effect of heterogeneity, University of Strathclyde., 2010.

765 Moir, H., Lunn, R. J., Shipton, Z. K. and Kirkpatrick, J. D.: Simulating brittle fault evolution from
766 networks of pre-existing joints within crystalline rock, J. Struct. Geol., 32(11), 1742–1753,
767 doi:10.1016/j.jsg.2009.08.016, 2010.

768 Monaghan, A. .: The Carboniferous shales of the Midland Valley of Scotland : geology and resource
769 estimation, British Geological Survey for Department of Energy and Climate Change, London, UK.,
770 2014.

771 Mykura, W.: White trap in some Ayrshire Coals, Scottish J. Geol., 1(2), 176–184,
772 doi:10.1144/sjg01020176, 1965.

773 Nasseri, M. H. B., Tatone, B. S. A., Grasselli, G. and Young, R. P.: Fracture toughness and fracture
774 roughness interrelationship in thermally treated westerly granite, Pure Appl. Geophys., 166(5–7), 801–
775 822, doi:10.1007/s00024-009-0476-3, 2009.

776 Nicol, A., Watterson, J., Walsh, J. J. and Childs, C.: The shapes, major axis orientations and
777 displacement patterns of fault surfaces, J. Struct. Geol., 18(2–3), 235–248, doi:10.1016/S0191-
778 8141(96)80047-2, 1996.

779 Nixon, C.W., Sanderson, D.J., Dee, S.J., Bull, J.M., Humphreys, R.J., Swanson, M.H.: Fault
780 interactions and reactivation within a normal-fault network at Milne Point, Alaska, AAPG Bulletin,
781 98(10), 2081-2107 doi: 10.1306/04301413177, 2014.

782 Nyberg, B., Nixon, C. W. and Sanderson, D. J.: NetworkGT: A GIS tool for geometric and topological
783 analysis of two-dimensional fracture networks, Geosphere, 14(4), 1618–1634,
784 doi:10.1130/GES01595.1, 2018.

785 Nygård, R., Gutierrez, M., Bratli, R. K. and Høeg, K.: Brittle-ductile transition, shear failure and
786 leakage in shales and mudrocks, Mar. Pet. Geol., 23(2), 201–212, doi:10.1016/j.marpetgeo.2005.10.001,
787 2006.

788 O'Keefe, J. M. K., Bechtel, A., Christanis, K., Dai, S., DiMichele, W. A., Eble, C. F., Esterle, J. S.,
789 Mastalerz, M., Raymond, A. L., Valentim, B. V., Wagner, N. J., Ward, C. R. and Hower, J. C.: On the
790 fundamental difference between coal rank and coal type, Int. J. Coal Geol., 118, 58–87,
791 doi:10.1016/j.coal.2013.08.007, 2013.

792 Oliver, N. H. S. and Bons, P. D.: Mechanisms of fluid flow and fluid–rock interaction in fossil
793 metamorphic hydrothermal systems inferred from vein-wallrock patterns, geometry and microstructure,
794 Geofluids, 1(2), 137–162, doi:https://doi.org/10.1046/j.1468-8123.2001.00013.x, 2001.

795 Peacock, D. C. P.: The temporal relationship between joints and faults, J. Struct. Geol., 23(2–3), 329–
796 341, doi:10.1016/S0191-8141(00)00099-7, 2001.

797 Peacock, D. C. P. and Sanderson, D. J.: Structural analyses and fracture network characterisation: Seven
798 pillars of wisdom, Earth-Science Rev., 184(June), 13–28, doi:10.1016/j.earscirev.2018.06.006, 2018.

799 Peacock, D. C. P., Sanderson, D. J. and Rotevatn, A.: Relationships between fractures, J. Struct. Geol.,
800 106, 41–53, doi:10.1016/j.jsg.2017.11.010, 2018.

Peacock, D. C. P., Rotevatn, A. and Sanderson, D. J.: Brecciation driven by changes in fluid column heights, Terra Nov., 31(1), 76–81, doi:10.1111/ter.12371, 2019.

Pei, Y., Paton, D. A., Knipe, R. J. and Wu, K.: A review of fault sealing behaviour and its evaluation in siliciclastic rocks, Earth-Science Rev., 150, 121–138, doi:10.1016/j.earscirev.2015.07.011, 2015.

Priest, S. D. and Hudson, J. A.: Estimation of discontinuity spacing and trace length using scanline surveys, Int. J. Rock Mech. Min. Sci., 18(3), 183–197, doi:10.1016/0148-9062(81)90973-6, 1981.

Ramsay, J. G.: The crack-seal mechanism of rock deformation, Nature, 284(5752), 135–139, 1980.

Ranalli, G. and Yin, Z. M.: Critical stress difference and orientation of faults in rocks with strength anisotropies: the two-dimensional case, J. Struct. Geol., 12(8), 1067–1071, doi:10.1016/0191-8141(90)90102-5, 1990.

Read, W. A., Browne, M. A. ., Stephenson, D. and Upton, B. J. .: Carboniferous, in The Geology of Scotland, edited by N. H. Trewin, pp. 251–300, Geological Society, London, London, UK., 2002.

Reed, B. W., Kumar, M., Minich, R. W. and Rudd, R. E.: Fracture roughness scaling and its correlation with grain boundary network structure, Acta Mater., 56(13), 3278–3289, doi:10.1016/j.actamat.2008.03.019, 2008.

Rippon, J., Read, W. A. and Park, R. G.: The Ochil Fault and the Kincardine basin: Key structures in the tectonic evolution of the Midland Valley of Scotland, J. Geol. Soc. London., 153(4), 573–587, doi:10.1144/gsjgs.153.4.0573, 1996.

Rippon, J. H., Ellison, R. A. and Gayer, R. A.: A review of joints (cleats) in British Carboniferous coals : indicators of palaeostress orientation, Proc. Yorksh. Geol. Soc., 56(Part 1), 15–30, https://doi.org/10.1144/pygs.56.1.15, 2006.

Ritchie, J. D., Johnson, H., Browne, M. A. E. and Monaghan, A. A.: Late Devonian-Carboniferous tectonic evolution within the Firth of Forth, Midland Valley: As revealed from 2D seismic reflection data, Scottish J. Geol., 39(2), 121–134, doi:10.1144/sjg39020121, 2003.

Roche, V., Homberg, C. and Rocher, M.: Fault nucleation, restriction, and aspect ratio in layered sections: Quantification of the strength and stiffness roles using numerical modeling, J. Geophys. Res. Solid Earth, 118, 4446–4460, https://doi.org/10.1002/jgrb.50279, 2013.

Rohrbaugh, J. B., Dunne, W. M. and Mauldon, M.: Estimating fracture trace intensity, density, and mean length using circular scan lines and windows, Am. Assoc. Pet. Geol. Bull., 86(12), 2089–2104, doi:10.1306/61EEDE0E-173E-11D7-8645000102C1865D, 2002.

De Rosa, S., Shipton, Z., Lunn, R., Kremer, Y. and Murry, T.: Along-strike fault core thickness variations of a fault in poorly lithified sediments, Miri (Malaysia), J. Struct. Geol., 116, 189–206, doi:https://doi.org/10.1016/j.jsg.2018.08.012, 2018.

Sanderson, D. J.: Field-based structural studies as analogues to sub-surface reservoirs, in Geological Society Special Publication, vol. 436, pp. 207–217, Geological Society of London., https://doi.org/10.1144/SP436.5, 2015.

Sanderson, D. J. and Nixon, C. W.: The use of topology in fracture network characterization, J. Struct. Geol., 72, 55–66, doi:10.1016/j.jsg.2015.01.005, 2015.

Sanderson, D. J. and Nixon, C. W.: Topology, connectivity and percolation in fracture networks, J. Struct. Geol., 115(August 2016), 167–177, doi:10.1016/j.jsg.2018.07.011, 2018.

Scheiber, T., Fredin, O., Viola, G., Jarna, A., Gasser, D. and Łapińska-viola, R.: Manual extraction of bedrock lineaments from high-resolution LiDAR data : methodological bias and human perception, GFF, 137(4), doi:10.1080/11035897.2015.1085434, 2015.

Schmatz, J., Vrolijk, P. J. and Urai, J. L.: Clay smear in normal fault zones - The effect of multilayers and clay cementation in water-saturated model experiments, J. Struct. Geol., 32(11), 1834–1849, doi:10.1016/j.jsg.2009.12.006, 2010.

Schöpfer, M. P. J., Childs, C. and Walsh, J. J.: Localisation of normal faults in multilayer sequences, J. Struct. Geol., 28(5), 816–833, doi:10.1016/j.jsg.2006.02.003, 2006.

Schöpfer, M. P. J., Childs, C. and Walsh, J. J.: Two-dimensional distinct element modeling of the structure and growth of normal faults in multilayer sequences: 2. Impact of confining pressure and strength contrast on fault zone geometry and growth, J. Geophys. Res. Solid Earth, 112(10), doi:10.1029/2006JB004903, 2007.

Schöpfer, M. P. J., Childs, C., Walsh, J. J. and Manzocchi, T.: Evolution of the internal structure of fault zones in three-dimensional numerical models of normal faults, Tectonophysics, 666, 158–163, doi:10.1016/j.tecto.2015.11.003, 2016.

Shang, J., Hencher, S. R. and West, L. J.: Tensile Strength of Geological Discontinuities Including Incipient Bedding, Rock Joints and Mineral Veins, Rock Mech. Rock Eng., 49, 4213–4225, doi:https://doi.org/10.1007/s00603-016-1041-x, 2016.

Sibson, R. H.: Conditions for fault-valve behaviour, edited by R. J. Knipe and E. . Rutter, Geol. Soc. London, Spec. Publ., 54(1), 15–28, doi:10.1144/GSL.SP.1990.054.01.02, 1990.

Sibson, R. H.: Implications of fault-valve behaviour for rupture nucleation and recurrence, Tectonophysics, 211(1–4), 283–293, doi:10.1016/0040-1951(92)90065-E, 1992.

Sibson, R. H.: Structural permeability of fluid-driven fault-fracture meshes, J. Struct. Geol., 18(8), 1031–1042, doi:10.1016/0191-8141(96)00032-6, 1996.

Skurtveit, E., Torabi, A., Alikarami, R. and Braathen, A.: Fault baffle to conduit developments: reactivation and calcite cementation of deformation band fault in aeolian sandstone, Pet. Geosci., 21(1), 3–16, doi:https://doi.org/10.1144/petgeo2014-031, 2015.

Soden, A. M. and Shipton, Z. K.: Dilational fault zone architecture in a welded ignimbrite: The importance of mechanical stratigraphy, J. Struct. Geol., 51, 156–166, doi:10.1016/j.jsg.2013.02.001, 2013.

Soliva, R. and Benedicto, A.: Geometry, scaling relations and spacing of vertically restricted normal faults, J. Struct. Geol., 27(2), 317–325, doi:10.1016/j.jsg.2004.08.010, 2005.

Soper, N. J., Strachan, R. A., Holdsworth, R. E., Gayer, R. A. and Greiling, R. O.: Sinistral transpression and the Silurian closure of Iapetus, J. Geol. Soc. London, 149, 871–880, doi:https://doi.org/10.1144/gsjgs.149.6.0871, 1992.

Thomas, L.: Coal Geology, Second., Wiley-Blackwell, Chichester., 2013.

Tsang, Y. W. and Witherspoon, P. A.: The dependence of fracture mechanical and fluid flow properties on fracture roughness and sample size, J. Geophys. Res., 88(B3), 2359, doi:10.1029/JB088iB03p02359, 1983.

Turichshev, A. and Hadjigeorgiou, J.: Triaxial compression experiments on intact veined andesite, Int. J. Rock Mech. Min. Sci., 86, 179–193, doi:https://doi.org/10.1016/j.ijrmms.2016.04.012, 2016.

Turichshev, A. and Hadjigeorgiou, J.: Quantifying the effects of vein mineralogy, thickness, and orientation on the strength of intact veined rock, Eng. Geol., 226, 199–208, doi:https://doi.org/10.1016/j.enggeo.2017.06.009, 2017.

Underhill, J. R., Monaghan, A. A. and Browne, M. A. E.: Controls on structural styles, basin development and petroleum prospectivity in the Midland Valley of Scotland, Mar. Pet. Geol., 25(10), 1000–1022, doi:10.1016/j.marpetgeo.2007.12.002, 2008.

Virgo, S., Abe, S. and Urai, J. L.: Extension fracture propagation in rocks with veins: Insight into the crack-seal process using Discrete Element Method modeling, J. Geophys. Res. Solid Earth, 118(10), 5236–5251, doi:https://doi.org/10.1002/2013JB010540, 2013.

Virgo, S., Abe, S. and Urai, J. L.: The evolution of crack seal vein and fracture networks in an evolving stress field: Insights from Discrete Element Models of fracture sealing, J. Geophys. Res. Solid Earth, 119(12), 8709–8727, doi:https://doi.org/10.1002/2014JB011520, 2014.

Walsh, J. J., Nicol, A. and Childs, C.: An alternative model for the growth of faults, J. Struct. Geol., 24(11), 1669–1675, doi:10.1016/S0191-8141(01)00165-1, 2002.

Wilkins, S. J. and Gross, M. R.: Normal fault growth in layered rocks at Split Mountain, Utah: Influence of mechanical stratigraphy on dip linkage, fault restriction and fault scaling, J. Struct. Geol., 24(9), 1413–1429, doi:10.1016/S0191-8141(01)00154-7, 2002.

Wilkins, S. J., Gross, M. R., Wacker, M., Eyal, Y. and Engelder, T.: Faulted joints: Kinematics, displacement-length scaling relations and criteria for their identification, J. Struct. Geol., 23(2–3), 315–327, doi:10.1016/S0191-8141(00)00098-5, 2001.

Woodcock, N. H. and Mort, K.: Classification of fault breccias and related fault rocks, Geol. Mag., 145(3), 435–440, doi:10.1017/S0016756808004883, 2008.

Yielding, G., Lykakis, N. and Underhill, J. R.: The role of stratigraphic juxtaposition for seal integrity in proven CO2 fault-bound traps of the Southern North Sea, Pet. Geosci., 17(2), 193–203, doi:10.1144/1354-0793/10-026, 2011.

Yuan, Y. S., Jin, Z. J., Zhou, Y., Liu, J. X., Li, S. J. and Liu, Q. Y.: Burial depth interval of the shale brittle–ductile transition zone and its implications in shale gas exploration and production, Pet. Sci.,

14(4), 637–647, doi:10.1007/s12182-017-0189-7, 2017.

van der Zee, W. and Urai, J. L.: Processes of normal fault evolution in a siliciclastic sequence: A case study from Miri, Sarawak, Malaysia, J. Struct. Geol., 27(12), 2281–2300, doi:10.1016/j.jsg.2005.07.006, 2005.

Vitale, S., Dati, F., Mazzoli, S., Ciarcia, S., Guerriero, V., Lannace, A.: Modes and timing of fracture network development in poly-deformed carbonate reservoir analogues, Mt. Chianello, southern Italy, J. Struct. Geol., 37(4), 223-235, doi: https://doi.org/10.1016/j.jsg.2012.01.005, 2012.

Zhao, G. and Johnson, A. M.: Sequence of deformations recorded in joints and faults, Arches National Park, Utah, J. Struct. Geol., 14(2), 225–236, doi:10.1016/0191-8141(92)90059-6, 1992.